Precambrian Research 425 (2025) 107828

Contents lists available at ScienceDirect

Precambrian Research

journal homepage: www.elsevier.com/locate/precamres

Age and structural evolution of the orogenic gold deposits in Kullaa, SW Finland: Implications for fluid activity and gold precipitation during evolving orogeny

Jaakko Kara [a,*], Jukka Manninen [a], Pietari Skyttä [a], Markku Väisänen [a], Hugh O'Brien [b], Kathryn Cutts [b], Paavo Nikkola [b]

[a] Department of Geography and Geology, University of Turku, Turku, Finland
[b] Geological Survey of Finland, Espoo, Finland

ARTICLE INFO

Keywords:
Orogenic gold
Svecofennian orogen
Age determination
Structural geology

ABSTRACT

We have studied two gold deposits, Välimäki and Kultakallio, located in SW Finland, to understand the interplay between gold precipitation, fluid activity and structural evolution within the Paleoproterozoic Svecofennian orogen. The Välimäki deposit is hosted by paragneisses characterised by pervasive silicification and the occurrence of foliation parallel quartz veins. The Kultakallio garnet-bearing gabbro shows two generations of quartz veins associated with arsenopyrite and graphite. Zircons from the leucosome within Välimäki yield an age of 1887 ± 4 Ma interpreted as the first metamorphic event (M1) associated with partial melting. In contrast, monazites of the same sample give bimodal ages at 1817 ± 7 Ma and 1794 ± 5 Ma both reflecting hydrothermal activity. *In-situ* zircon dating in Kultakallio yielded three age peaks at 1885 ± 4 Ma, 1859 ± 5 Ma and 1805 ± 7 Ma interpreted to represent magmatism, a secondary metamorphic event (M2) and hydrothermal activity, respectively. *In-situ* dating of Kultakallio titanites gives an age of 1786 ± 58 Ma and garnet an age of 1809 ± 470 Ma, which reflect the timing of the fluid activity. Based on hydrothermal ages, gold mineralising events at (I) 1815–1805 Ma and (II) 1795–1785 Ma are recognised in the study area. Stage I is related to the injection of foliation-parallel quartz veins and precipitation of arsenopyrite in which gold occurs as inclusions. Stage II is characterised by precipitation of gold associated with Te- and Bi-minerals, abundant graphite, remobilisation of pyrite and breakdown of arsenopyrite within the brittle-ductile transition zone. The NW-SE –oriented transpressional setting formed the NE-SW –oriented gold critical structures originally at 1.89–1.88 Ga (D2), which were later reactivated in the 1.83–1.78 Ga WNW-ESE transpressional setting (D3). The NW-SE trending crustal scale shear zones are suggested to act as first order structures whereas the NE-SW oriented strike-slip structures form the second order setting. In the target scale, foliation parallel and intersecting quartz veins and narrow shear zones represent the third order structures hosting the mineralisations. We suggest the driver for the fluid activity at ca. 1.80 Ga is lower crustal delamination during crustal extension in a tectonic switching cycle.

1. Introduction

Mineralisation is an output of diverse geological processes within a specific geological setting. To understand ore genesis, we must be able to recognise and characterise the processes leading to ore formation. One approach is to conduct integrated *in-situ* dating of several mineral species (e.g. zircon, monazite, titanite and garnet) which allows us to determine the relative and absolute timing(s) of processes related to the precipitation, emplacement and/or remobilisation of the ore (i.e. formation of the ore deposit). The strength of *in-situ* multimineral age determinations is not limited to the structural and mineralogical control of the dated minerals alone but also allows evaluation of the distinct response of the studied mineral species to the prevailing conditions (P, T, fluid activity and composition) during and after their crystallisation and potential (partial) recrystallisation. Such an approach is particularly important in complex Precambrian terrains where direct constraints over the geological evolution using e.g. stratigraphy or petrography is critically limited or non-existent.

* Corresponding author.
E-mail address: jkmkar@utu.fi (J. Kara).

https://doi.org/10.1016/j.precamres.2025.107828
Received 11 March 2025; Received in revised form 12 May 2025; Accepted 24 May 2025
Available online 27 May 2025

The Paleoproterozoic Svecofennian orogen in Finland (Fig. 1A) is characterised both by a complex and prolonged evolution (1.96–1.77 Ga) and the presence of numerous structurally controlled gold occurrences, the majority of which classify as orogenic gold deposits (e.g., Eilu et al., 2003; Eilu, 2012, Saalmann et al., 2009, 2010). In northern Finland (the Central Lapland Greenstone Belt), *in-situ* age determination has shown that the precipitation of gold during the Svecofennian evolution occurred in two separate events at 1.91–1.87 Ga and 1.82–1.77 Ga (Molnár et al., 2018). In contrast, the few available contributions from the Häme belt in SW Finland indicate a more limited duration of gold mineralising event(s) at 1.83–1.78 Ga, when structural control was provided by specifically oriented shear zones and faults that formed in response to WNW-ESE crustal shortening (Saalmann, 2007 ; Saalmann et al., 2009, 2010). Moreover, at least two separate gold precipitating events, with poorly resolved timing have been recognised from the mineralogical association of gold in several deposits in SW Finland (Lehto and Kärkkäinen, 2006; Kärkkäinen et al., 2012, 2015, 2016). However, the Svecofennian orogen in SW Finland is composed of four E-W trending volcano-sedimentary belts, which are distinctive with respect to the lithological composition, timing and conditions of the metamorphic events, timing and volume of magmatism, and deformation style (e.g., Lahtinen et al., 2005; Nironen, 2017; Hölttä and Heilimo, 2017; Kara et al., 2021). For these reasons, the validity of the results by Saalmann et al. (2009) to the other supracrustal belts remains untested. This is true also for the gold deposits in Kullaa, the area of the present study, which is located in the western part of the high metamorphic grade Pirkanmaa belt that occurs to the north of the medium-grade Häme belt (Fig. 1B).

The purpose of this investigation is (i) to conduct a geochronological-structural characterisation of the Kullaa district and the contained gold mineralisation, (ii) further test whether the results by Saalmann et al. (2009) are more universally applicable beyond the Häme belt, and (iii) eventually propose models that explain the tectonic setting and geological controls of the fluid pulses that penetrated large volumes of the Svecofennian bedrock and resulted in the deposition of numerous orogenic gold deposits. The characterisation work involves determining ages of the gold precipitating fluid activity, the host-rock to the mineralisation and the metamorphic peak. These will be used to elucidate the character and timing of the structures controlling the mineralisation. The principal methods used in this work are field mapping, subsequent analysis of field and geophysical data, and U-Pb age determinations on zircon, monazite, titanite and garnet.

2. Geological setting

2.1. Svecofennian orogen

The Fennoscandian shield, comprising roughly half of the East European Craton, hosts four main domains: the Archean (3.5–2.5 Ga), Svecofennian (1.95–1.79 Ga), Transscandinavian Igneous Belt (TIB; 1.81–1.65 Ga) and Sveconorwegian (1140–960 Ma; e.g., Lahtinen et al., 2023). The Paleoproterozoic Svecofennian orogen formed as a consequence of accretionary processes (e.g., Lahtinen et al., 2009). In Finland, the Svecofennian Province is further divided into the Southern Svecofennia and the Northern Svecofennia Subprovinces, which represent the main arc complexes (Kohonen et al. 2021; Fig. 1A). The Svecofennian rocks are separated from the Archean rocks in the NE by a NW-SE −trending complex suture zone. For more detailed description, see e.g., Gaál and Gorbatschev, (1987), Nironen (1997) and Lahtinen et al. (2005).

Four E-W trending volcano-sedimentary belts occur within the Svecofennian Province in SW Finland: Tampere, Pirkanmaa, Häme and Uusimaa belts of which the first two belong to the Northern Svecofennia Subprovince and the last two to the Southern Svecofennia Subprovince

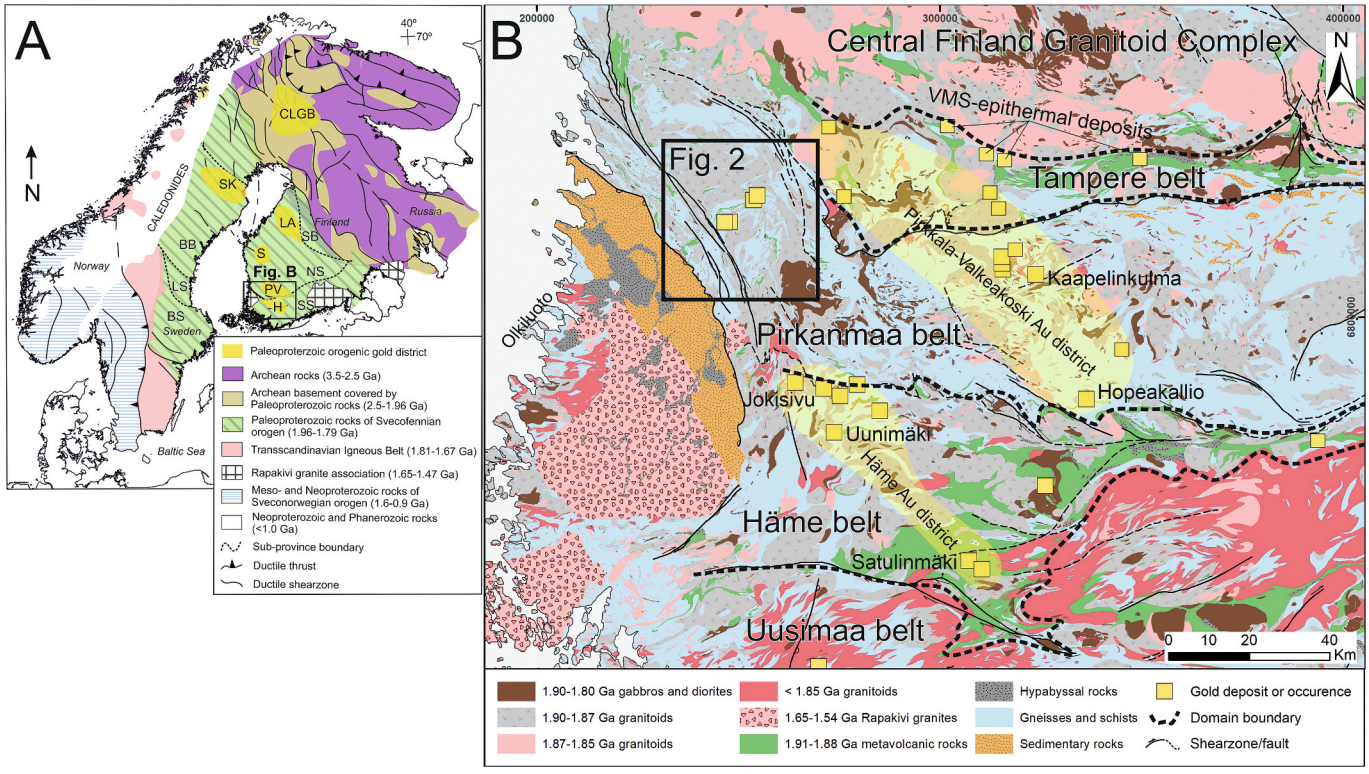

Fig. 1. A. Generalised overview of the Fennoscandian Shield with major Paleoproterozoic gold districts indicated, modified after Koistinen et al. (2001). SB = Savo belt, NS = Northern Svecofennia Subprovince, SS = Southern Svecofennia Subprovince CLGB = The Central Lapland Greenstone Belt, SK = Skellefte, LA = Laivakangas, S = Seinäjoki, PV = Pirkkala-Valkeakoski, H = Häme. B. Generalised lithological map of the study area and SW Finland with gold occurrences. Geological data modified after Bedrock of Finland – DigiKP (2024).

(Fig. 1B). The medium-grade Tampere belt is situated north of the Pirkanmaa belt and is characterised by volcanic rocks formed in a volcanic arc environment 1.91–1.89 Ga ago (Kähkönen, 2005; Kara et al., 2022). The Pirkanmaa belt is interpreted to represent the accretionary prism of the same complex, consisting mostly of migmatites and gneisses of turbiditic origin together with 1.89–1.87 Ga plutonic rocks, predominantly granodioritic in composition (Lahtinen et al., 2009). The Pirkanmaa belt was subjected to complex deformation (Kilpeläinen, 1998) involving early thrusting and associated sub-horizontal folding, followed by extension and almost synchronous upright folding in a low-P, high-T −environment at upper amphibole facies (Hölttä and Heilimo, 2017), peaking at 1.88 Ga (Mouri et al., 1999). The internal structures of the Pirkanmaa belt in the area south of the Tampere belt are characterised by bedding-parallel foliations, which have been folded into E-trending upright folds with sub-horizontal axes. Faults within the Pirkanmaa belt occur as conjugate sets with respect to the E-trending axial planes and the thrust-type contact with the Tampere belt (Kilpeläinen, 1998). The border between the Pirkanmaa belt and Tampere belt in the north displays both gradual and fault-controlled changes. Kilpeläinen (1998) and Nironen (1989) described thrust faulting with S-side-up −kinematics. The border between the Pirkanmaa and Häme belts is interpreted to represent the suture zone between the two crustal Subprovinces (Korsman et al., 1997; Kohonen et al. 2021). The Häme belt was mainly formed at 1.89–1.87 Ga and consists of volcanic and sedimentary rocks (Lahtinen, 1996; Kähkönen, 2005) that were metamorphosed at amphibolite facies (Hölttä and Heilimo, 2017) and intruded by 1.89–1.87 Ga gabbros, diorites, granodiorites and tonalites (Suominen, 1988; Kähkönen, 2005; Saalmann et al., 2010; Tiainen et al., 2013).

2.2. Kullaa area

The study area is located within the Pomarkku block, which is the western continuation of the Pirkanmaa belt located between the Satakunta sandstone basin and the Central Finland Granitoid Complex (Fig. 1B and 2). The Pomarkku block is dominated by plutonic units with granodioritic to dioritic compositions (Fig. 2). Migmatised supracrustal sedimentary units, typical for the Pirkanmaa belt, along with minor mafic to intermediate volcanic units are present. The metamorphic grade is typically upper amphibolite facies (Hölttä and Heilimo, 2017), while the timing of the peak metamorphism is unknown. Earlier studies with structural emphasis (Pietikäinen, 1994; Pajunen et al., 2008) focused on the regional structural evolution with no previous studies concerning the gold-critical structures.

The Pomarkku block is bordered by the crustal-scale Kynsikangas shear zone (KySZ) in the SW and the Kankaanpää shear zone (KaSZ) in the NE (Pietikäinen, 1994; Pajunen et al., 2008; Fig. 2). Reimers et al. (2018) concluded that deformation within the KySZ was partitioned into two different deformation regimes: i) A NW-SE oriented transpressional ductile regime that formed the map-scale structures in the KySZ and ii) regime related to more brittle E-W compression, which caused localised thrusting of the central KySZ segment upon its eastern segment. Structures along the SW margin of Pomarkku block were affected by the drag of shearing from the KySZ during NW-SE −oriented transpressional regime (Reimers et al., 2018). The KaSZ along the NE margin of the Pomarkku block displays lineations plunging gently towards NE and oblique dextral-reverse kinematics (Pajunen et al., 2008). The internal structures of the Pomarkku block are characterized by E-W trending foliations and axial planes, and north-verging folds in the northern part of the block shifting to NE-SW trends and vertical to subvertical axial planes in the southern part of the study area.

2.3. Overview of Paleoproterozoic orogenic gold mineralisation in the Fennoscandian shield

2.3.1. Major gold districts

Several Paleoproterozoic gold districts are recognised in the Fennoscandian shield of which the most notable are the Central Lapland Greenstone Belt (CLGB), Skellefte, Laivakangas, Seinäjoki, Pirkkala-Valkeakoski and Häme Au-districts (Fig. 1A). At least two major episodes of hydrothermal activity and gold precipitation are suggested within the CLGB (Molnár et al., 2018). This includes an early-stage refractory gold mineralisation taking place between 1916 and 1870 Ma (Molnár et al., 2018), which is associated with structurally controlled fluid flow along N-S oriented strike-slip faults (Hölttä et al., 2007; Molnár et al., 2018). The late-stage mineralisation with free gold in N-S and NW-SE oriented carbonate-quartz veins is characterised by sulphides and Bi-minerals and is dated between 1820 and 1770 Ma (Mänttäri, 1995; Hölttä et al., 2007; Molnár et al., 2018, 2019). The late-stage mineralisation is similar to the gold deposits south of the well-known Skellefte VMS district in which refractory and free gold is hosted by arsenopyrite-bearing quartz veins (Eilu et al., 2003; Bark and Weihed, 2007). The majority of the deposits in the area are structurally associated with ~ N-S striking, steeply dipping shear zones that were active roughly around 1.8 Ga during E-W shortening (Bark and Weihed, 2012).

Neither the age of the mineralisations nor the structural evolution of the deposits in Laivakangas, Seinäjoki and Pirkkala-Valkeakoski Au-districts have been studied in detail, but they share similarities with the aforementioned deposits. The Laivakangas Au district is characterised by deposits of Au-only and Au with atypical (Cu, Co, Ni) metal association and both deposit styles are hosted by shear zones (Eilu, 2012; Hector et al., 2023). Two gold precipitating events are identified in the deposits: an older As-Au mineralising event is suggested to occur near peak metamorphism and a younger Cu-Au + sulphide event during the retrograde stage (Hector et al., 2023). The Seinäjoki Au district hosts several small gold occurrences, which differ from the gold mineralisations elsewhere due to their high antimony content, in some cases making Sb a major commodity (Eilu et al., 2003; Isomaa et al., 2010). Free gold is situated in narrow E-W to NW-SE oriented quartz +/- tourmaline veins (Akkerman, 2015). Several structurally controlled gold deposits occur within the Pirkkala-Valkeakoski Au district in which gold is hosted by en echelon quartz veins within narrow shear zones (Eilu, 2012).

Saalmann et al., (2009) attributed the formation of the Jokisivu and Satulinmäki mineralisations, in the Häme gold district, to WNW-ESE oriented sub-horizontal shortening and dextral shearing in brittle-ductile boundary conditions that prevailed at 1.83–1.79 Ga. The controlling structures are WSW-ENE to SW-NE dextral shear zones and NW-SE oriented faults. Similar steep to sub-vertical NW-SE trending high-strain zones controlled the fluid flow in the Uunimäki deposit but the gold precipitated in the 4th order fracture network occurring along the boundary of the high and low-strain domains (Kara et al., 2021). The WSW-ENE structures are also recognised in the Uunimäki area, but these are interpreted as channels that facilitated the fluid ascent from depth.

2.3.2. Kullaa gold occurrences

The Kullaa area hosts four known gold targets: Välimäki, Kultakallio, Saarijärvi and Silmusuo, with the first two selected for closer study (Fig. 2). The Välimäki target is hosted by migmatised paragneisses and hornblende gneisses characterised by pervasive silicification and occurrence of thin quartz veins parallel to the foliation. Two quartz vein types can be detected in the area: i) folded and foliation parallel barren veins associated with leucosomes and ii) arsenopyrite bearing thin foliation parallel veins (Kärkkäinen et al., 2012). The gold-bearing quartz veins are hosted by narrow (a few centimetres to a few meters wide) shear zones and their alteration halos are characterised by the presence of garnet, quartz veins, biotite, arsenopyrite and pyrite. In addition to the quartz veins, gold is present in shear related sulphide and biotite veins (Lehto & Kärkkäinen, 2006; Kärkkäinen et al., 2012). Likewise, two generations of quartz veins have been detected from the Kultakallio garnet-bearing gabbro or gabbroic diorite. The older generation veins are sub-parallel with the host-rock fabric whereas the

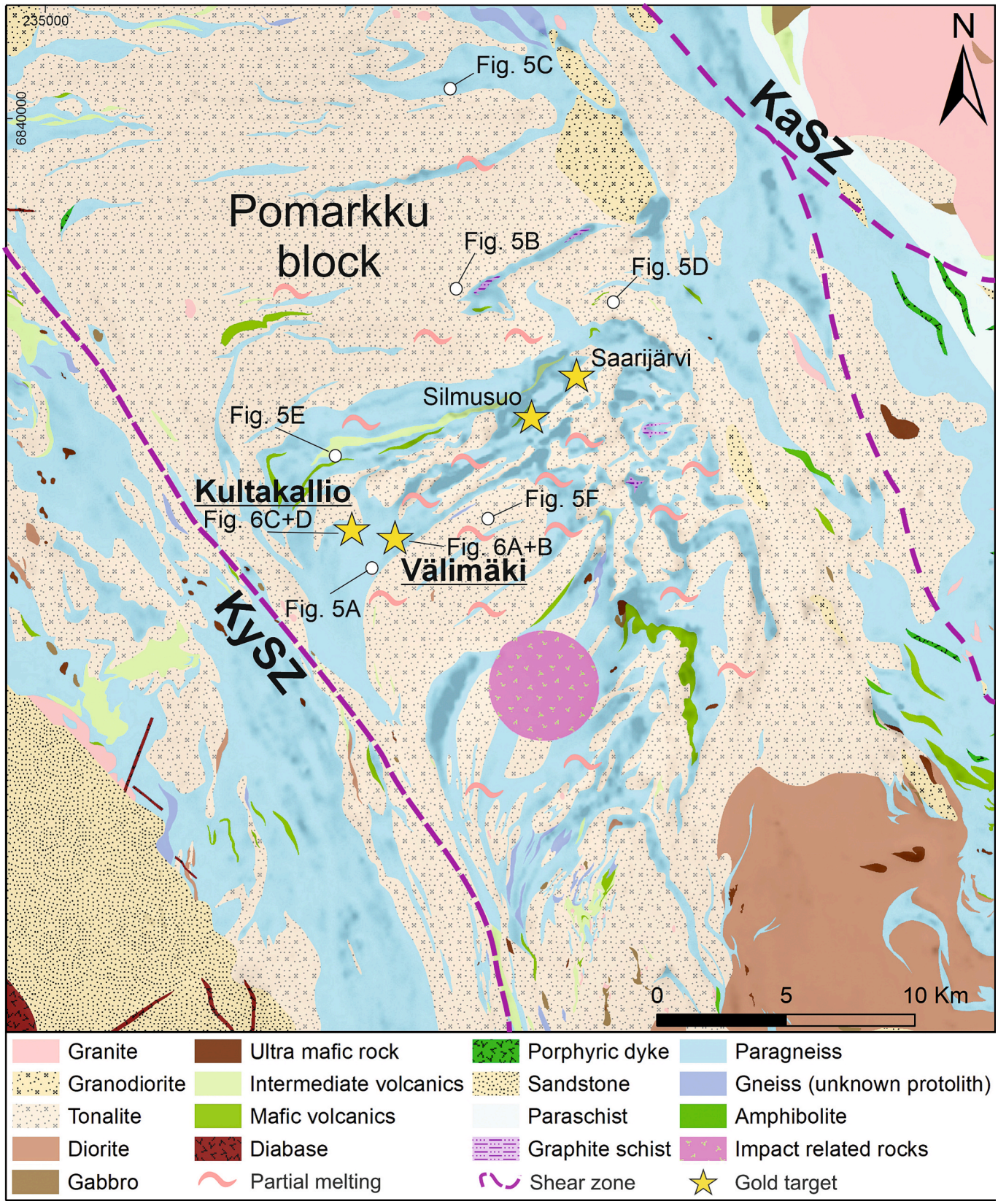

Fig. 2. Lithological map of the study area with gold targets, main shear zones and figure locations indicated. Aeromagnetic low-altitude grayscale map as a background ©Geological Survey of Finland. KySZ = Kynsikangas Shear Zone, KaSZ = Kankaanpää Shear Zone. Modified after Bedrock of Finland – DigiKP (2024).

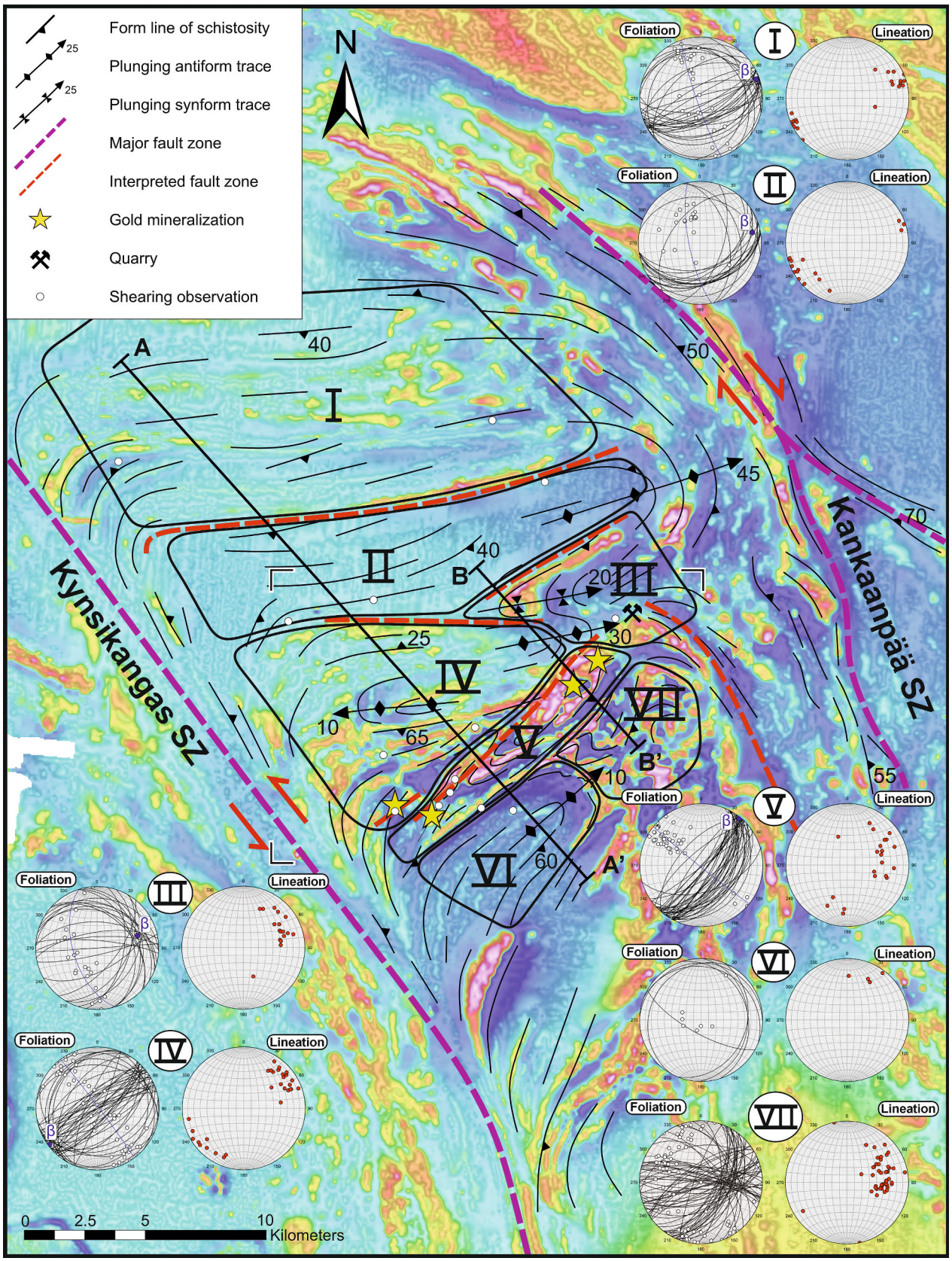

Fig. 3. Form line map of the study area with tilt derivate (TDR) processed aeromagnetic map ©Geological Survey of Finland on the background. Subdivision into structural domains presented with lower hemisphere stereographic projections from each structural domain displaying planar (foliation) and linear (lineation and fold axis) features along with statistical β axis. Black line indicates the location of cross sections A-A' and B-B' from the study area and the corners of the detailed form line map (Fig. 4A) have been marked. Locations of illustrated shearing observations have been marked.

younger veins cut all the previous structures. Gold occurs in both vein types (Kärkkäinen et al., 2016). Gold usually is in native form in both locations and is associated with arsenopyrite-pyrite ± chalcopyrite and locally also with Bi- and Te-minerals (Kärkkäinen et al., 2012). Precipitation of gold has been suggested to occur in two phases or during a single phase with a relatively long time span in the whole Kullaa area (Kärkkäinen et al., 2012, 2016). The early phase comprises Ag-bearing gold which occurs as inclusions in arsenopyrite, whereas the late phase of gold is usually related to Te-Bi minerals or mobilised fault-fill pyrite, ilmenite and chalcopyrite (Kärkkäinen et al., 2012). Garnet is usually absent in gold mineralised and quartz- or arsenopyrite-rich zones but instead borders these zones (Kärkkäinen et al., 2016).

Both the Välimäki and Kultakallio targets have been previously drilled by the Geological Survey of Finland (GTK). Data from a total of 14 unoriented drill holes from the Välimäki prospect indicate that gold mineralisation is associated with thin quartz veins, located in narrow, foliation-parallel shear zones (Fig. 6A; Lehto & Kärkkäinen, 2006). These gold-critical zones are narrow and scattered in nature with the highest gold contents at 12.7 ppm (R309, 15.00–16.00 m) and 13.9 ppm (R309, 21.00–22.00 m) (Lehto & Kärkkäinen, 2006). In the Kultakallio prospect, eight drill holes (R318–R325) totalling at 517.50 m were drilled during previous studies (Kärkkäinen et al., 2016). The Kultakallio drillholes (Fig. 6D) display shearing with mylonitic fabric, and breccia zones occurring parallel to the core in the SSE-plunging holes R318 and 319 (Kärkkäinen et al., 2016).

3. Methods

A full description of the methods used is available in the online supplementary material Electronic Appendix A and only the most relevant information is summarised here. The bedrock mapping was focused on observing those linear and planar features that have specific relevance to the deformation zones, fold geometries and apparent strain variations. Two targets were selected for age determinations: Kultakallio and Välimäki. A standard mineral separation procedure was conducted on the Välimäki granitic leucosome sample and zircons and monazites were recovered. Five polished thin sections were prepared from Kultakallio gabbro. The thin sections were imaged by a Hitachi SU3900 Low Vacuum Scanning Electron Microscope (LV-SEM), and the dateable minerals were identified using AZtec Software by Oxford Instruments. The epoxy mount was imagined by a JEOL TM JSM-7100F Field Emission Scanning Electron Microscope (FE-SEM). SEM-imaging was conducted at the Geological Survey of Finland (GTK). This was followed by the zircon, monazite, titanite and garnet U-Pb isotope age determinations using a Nu Plasma AttoM LA-SC-ICP-MS at GTK. The dated garnet grain was mapped on the polished thin section off-cutt by a Bruker M4 Tornado micro-XRF at the University of Turku.

4. Results

4.1. Lithology and regional structure

The study area is dominated by granodioritic to dioritic plutonic rocks, gneissic sedimentary rocks including migmatites, and minor intermediate to mafic volcanic rocks (Fig. 2). Pegmatitic dikes are associated with localised shearing or domains with a higher degree of migmatisation, which shows variation across the study area: in paragneisses the amount of partial melting is controlled by the composition of the protolith whereas in plutonic units present within the southern parts of the study area, the amount of partial melts increases with increasing strain (Fig. 2).

The study area is enveloped by the NW-trending shear zones KySZ and KaSZ, and the intervening volume is characterised by approximately orthogonal ENE-WSW structural trends, which are defined by variably dipping foliations and sub-horizontal to gently plunging mineral lineations and fold axes. Folding is synchronous or post-dates the metamorphic peak as shown by the folded leucosomes in para- and orthogneisses (Fig. 5A and B). Based on the variation in the character and orientation of the structural elements, the study area was divided into seven structural domains I – VII (Fig. 3).

Domains I & II: The northernmost Domains (I and II) are characterised by ENE-WSW trending planar structures, sub-horizontal mineral lineations and folds axes (Fig. 3). Domain I is homogeneous both lithologically and structurally; the dominant plutonic units display an intense, penetrative ENE-WSW trending L- to LS-tectonic fabric, where the lineations are sub-horizontal. The measured foliations in Domain I show steep SSE dips (dominant) and gentle northerly dips that are associated with open folds that have upright to steeply S-dipping axial surfaces and ENE and WSW sub-horizontally plunging fold axes.

In comparison with Domain I, the intensities of the linear and planar fabric in Domain II are less and more intense, respectively, with the highest apparent flattening strains observed in banded gneisses. The foliation in Domain II shows gentle to moderate SSE dips reflecting the structural position along the south-dipping limb of NNE-verging asymmetric folds or along the southern, gentler limb of folds in Domain I. The statistical fold axis in Domain II plunges sub-horizontally ENE and is hence sub-parallel with the observed mineral lineations. Domain II displays more minor shear bands across all the lithologies, whereas these features were predominantly localised into the banded gneisses in Domain I.

Field observations indicate that the proportion of partial melts increases towards the southern parts of the study area (Fig. 2), which also correlates with the increasing number of shearing observations from Domain I to Domain V. Partial melts are spatially associated with localised deformation in various localities in the study area (e.g. Fig. 5C). The melt-interconnectivity is affected by the lithology of the host-rock as compositional heterogeneity and homogeneity in the paragneisses and plutonic units, respectively, have resulted in lower and higher degrees of melt connectivity.

Domains III & IV represent large-scale fold structures with fold closures appearing at the map level (Figs. 3 and 4). Domain III delineates a gently ENE-plunging synform and a minor parallel antiform with axes that are typically parallel to the observed mineral lineations but may vary as e.g. within the vicinity of the KaSZ (Fig. 5D). The foliations have overall gentle dips and their poles cluster on a narrow belt-shaped girdle on the lower hemisphere projections, indicating that the observed folds are strictly cylindrical in character (Fig. 3). Domain IV is characterised by NE-SW structural trends, comprising a dominantly sub-vertical, and secondarily sub-horizontal foliation and sub-horizontally NE and SW-plunging mineral lineations. Foliation data are compatible with approximately upright folds with sub-horizontal, curvilinear fold axes (statistical axis plunges gently WSW), with a recognisable WSW-plunging antiform in the central part of the domain. Towards the southern margin of Domain IV which hosts the Kultakallio gold occurrence, the structures become dominantly sub-vertical and NE-SW trending.

Domain V hosts three of the known gold occurrences in the area. It is characterised by a linear NE-trending belt of positive magnetic anomalies (Fig. 4A) that truncate the ENE-WSW trends in the northern Domains. Domain V is bounded by two vertical strike-slip zones with apparent right lateral kinematics (Fig. 5E) that appear as continuous linear negative anomalies in aeromagnetic data (Fig. 4A). Structurally, Domain V displays the highest intensity and complexity within the study area. NE-SW trends containing SE-dipping foliation with variable dips are dominant (Fig. 3), whereas the linear features display more scatter, including a maxima with NE plunges and significant scatter towards N, E and SSW. Likely the scatter can be attributed to the complex internal structures and vertical flow of material. Contrasting to Domains I-III, the axial surfaces of folds in Domain V (and southern parts of Domain IV) are strictly vertical. Furthermore, two NE-SW −oriented oblique slip zones, occurring in-between the right-lateral strike-slip zones, are interpreted based on the plunge of the lineations and continuations on the

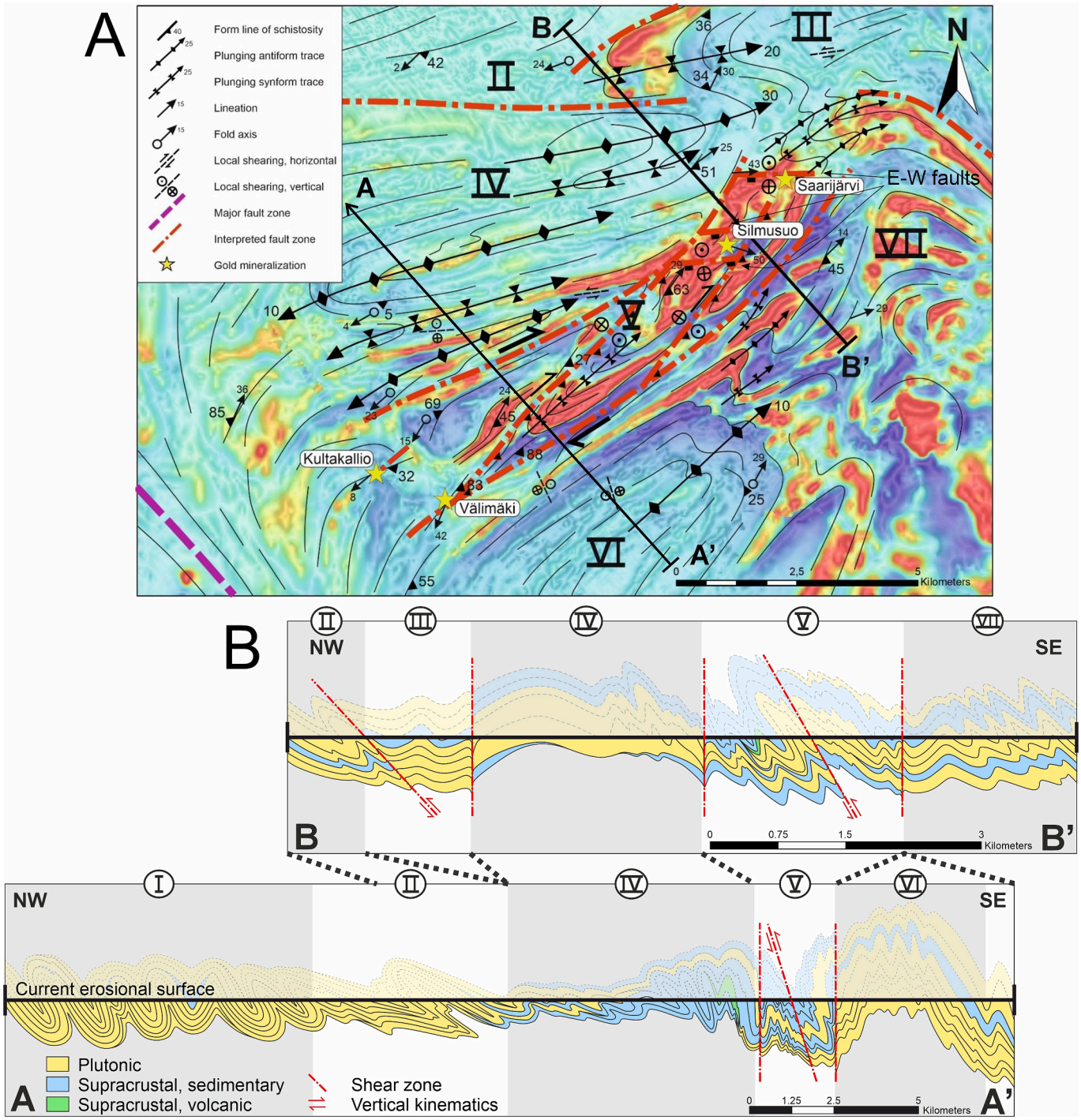

Fig. 4. A. A detailed form line map of the study area with aeromagnetic map ©Geological Survey of Finland. Black line indicates the positioning of cross sections A-A' and B-B' from the study area. B. Cross-sections A-A' and B-B'.

geophysical map (Fig. 4A) as well as the fluctuations in the strike of the foliation. A few E-W –trending discontinuities are present in the magnetic layers within the vicinity of the Silmusuo and Saarijärvi prospects (Figs. 3 and 4A), which may represent normal faulting, localised along releasing linkage structures between subparallel strike-slip and oblique-slip zones (Fig. 4A).

Domains VI & VII: Correlation of the structural data (although limited) with the signatures on the aeromagnetic maps point towards the presence of a gently NE-plunging anticline in Domain VI. For Domain VII, only a few structural observations were made, and hence pre-existing observations were used. Subsequent analysis revealed the presence of steeply to moderately east-dipping and steeply north-dipping foliations, the intersections of which define a moderately east-plunging statistical folds axis that is parallel with the orientation-maxima of the available mineral lineation data. The steeper plunge of the linear fabric is attributed to the close proximity to the KaSZ immediately west of this domain. Shear zones in Domains VI and VII are rare, and one of the few observed local shear zones shows N-S trends and normal kinematics (Fig. 5F) that deviate from the common regional trends.

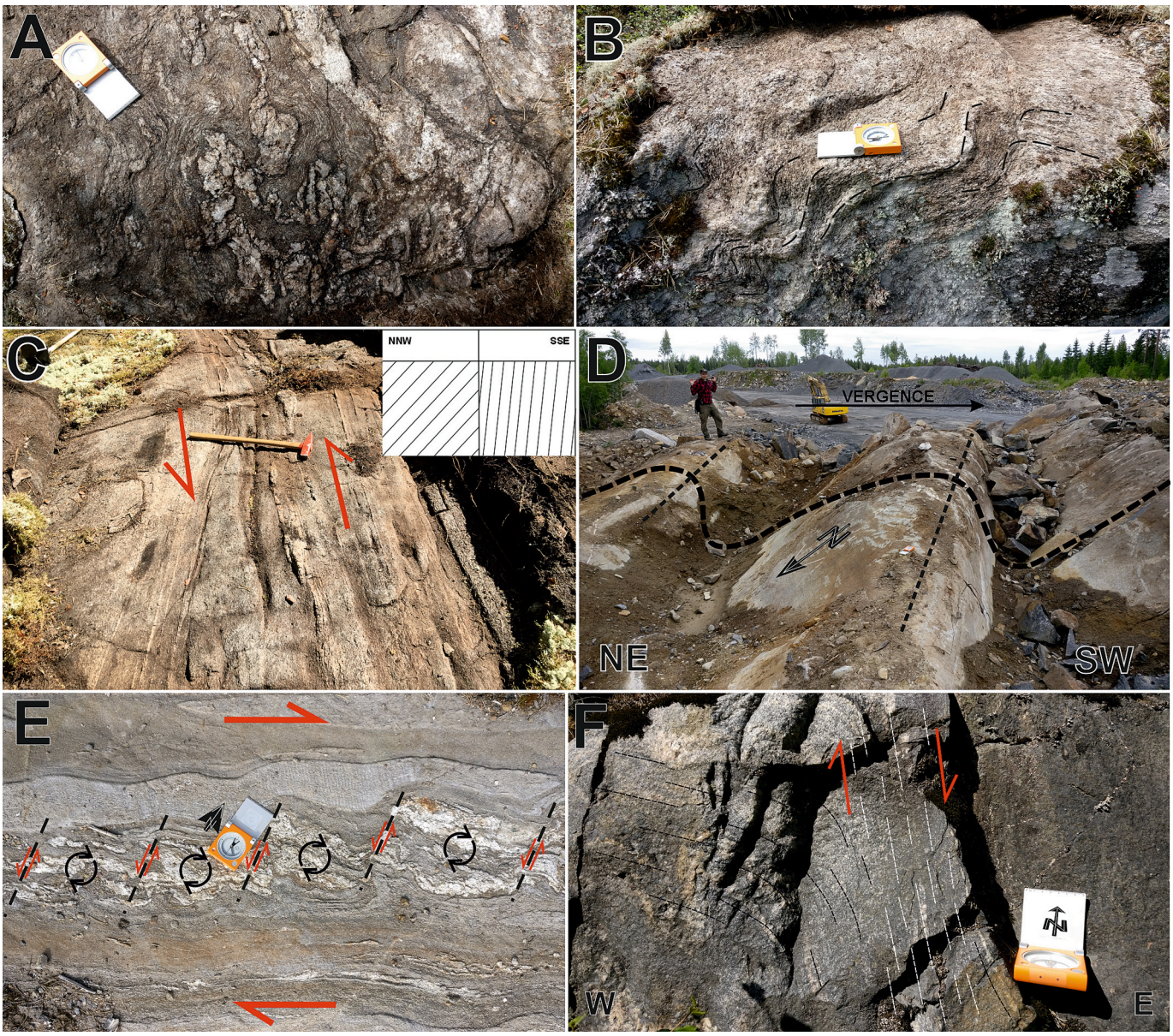

Fig. 5. Field photos from the study area. A. Folding in strongly migmatised paragneiss (Domain V). B. Folding in foliated and moderately migmatised orthogneiss with granodioritic protolith (Domain II). C. A shear zone displaying sub-vertical and moderately dipping foliation on the S and N side of the slip plane. Foliation deflection indicates sinistral and NNW-block-down (inset) kinematics. View towards ENE (Domain I), D. Asymmetrical folding of tonalite in the proximity of the KaSZ, vergence towards SW. Hinge lines marked by straight dashed line (Domain III), E. Clockwise rotation of more competent leucosome rich layers in a paragneiss host rock. Dextral shear sense, with antithetic shear band boudins with quartz filling in the N-S oriented shear bands (Domain V), F. A steeply east-dipping normal fault which caused the reorientation of the sub-horizontal foliation of the tonalitic protolith towards parallelism with the ductile shear zone. View towards N (Domain VI). A hammer (length of 60 cm), a compass (width of 7 cm) or geologist (height of 182 cm) for scale.

4.2. Structure and characteristics of the mineral occurrences

The four known gold prospects within the Pomarkku block occur within a distinct linear NE-SW trending magnetic anomaly (or its close vicinity), which is here attributed to a shear zone. The shear zone truncates the regionally dominant ENE-trending foliations, which in turn represent the folded intrusive and supracrustal rocks with penetrative LS-tectonic fabrics. However, the structural settings of the individual occurrences are mutually contrasting: The Kultakallio target is associated with a local NE-high-strain zone but located outside the major NE-SW deformation zone, comprises moderately dipping planar structures and sub-horizontal linear fabrics, which are characteristic for Domains I, II and IV. The planar structures within the Välimäki prospect are vertical whereas the linear features have gentle plunges. The Silmusuo prospect has moderately dipping planar, and steeply plunging linear features, respectively. The Saarijärvi target is located along the eastern continuity of the fault zone which hosts the Silmusuo prospect, and, based on pre-existing data, is dominated by planar structures with 60–70 degree dips towards NNW.

4.2.1. Välimäki

The Välimäki prospect is located close to the intersection of the larger ENE-trending dextral strike-slip and NE-trending reverse dips-slip shear zones that have been interpreted from the aeromagnetic signatures (Fig. 4A) and field observations. At the Välimäki outcrops, the observed main foliation is vertical and trends NE-SW (Fig. 6A), and mineral lineations have gentle plunges that are in agreement with the strike-slip character of the major shear zones in the area. Pelitic

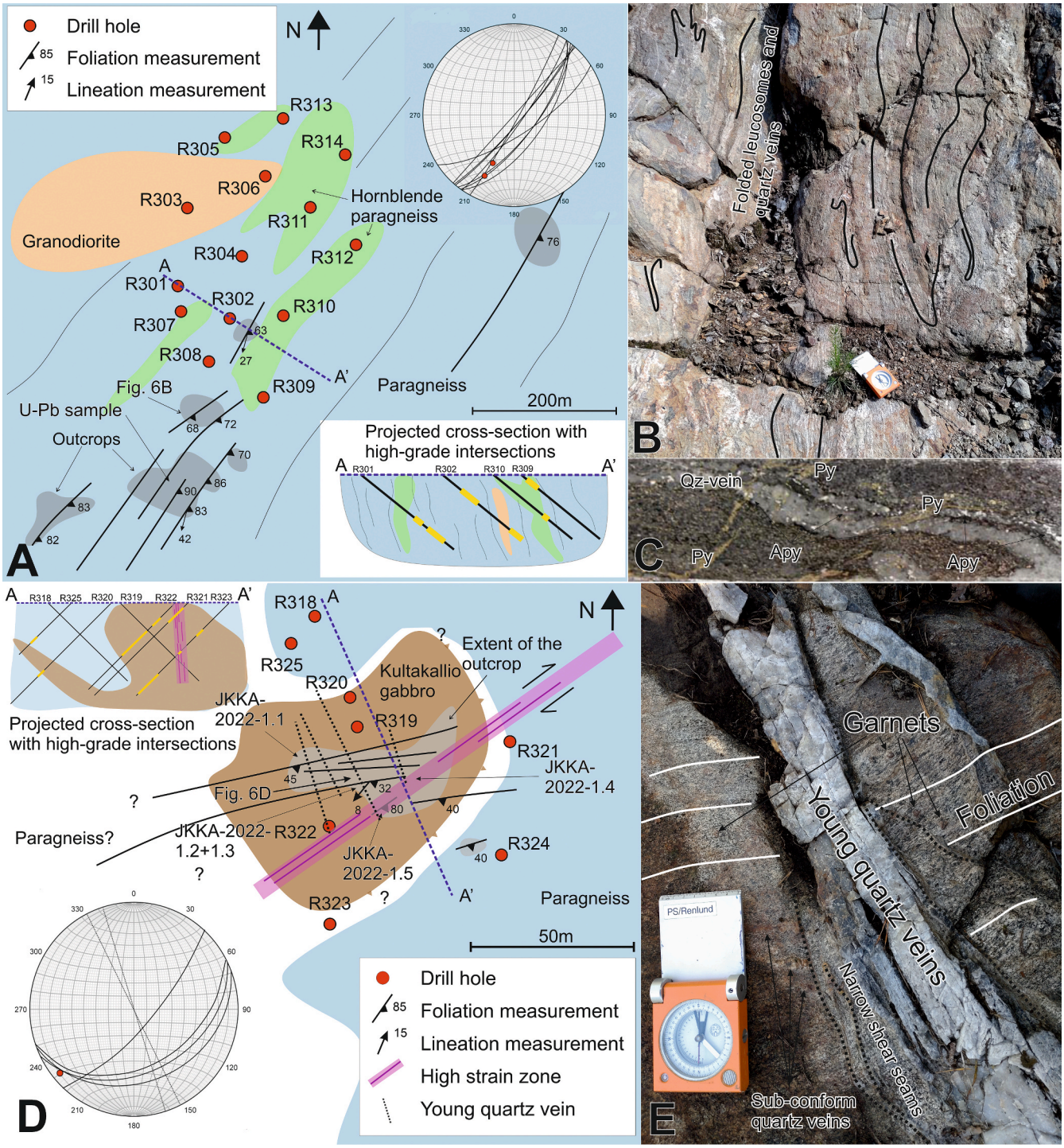

Fig. 6. Detailed lithological maps and structural interpretation of the Välimäki (A) and Kultakallio (D) prospects, including schematic cross-sections A-A' with projected high-grade gold drill hole intersections (data from Lehto and Kärkkäinen, 2006; Kärkkäinen et al., 2016) and lower hemisphere stereographic projections illustrating orientation distribution of the dominant foliation (grain shape fabrics; great circles) and mineral lineation (red dots). The existing drilling sites (collars) and observation sites indicated. B. Field example of a rusty and quartz vein-bearing biotite paragneiss from Välimäki. C. Arsenopyrite bearing quartz vein, which is cut by pyrite bearing shear seams. Photo of a drill core (40 mm thick) from Välimäki (adapted and modified after Kärkkäinen et al., 2012). E. Field example of the foliated, garnet and quartz vein-bearing Kultakallio gabbro, which is cut by a younger generation quartz vein. Qz = quartz, Apy = arsenopyrite, Py = pyrite. (For interpretation of the references to colour in this figure legend, the reader is referred to the web version of this article.)

sequences display crenulation of the main foliation (Fig. 7B) and tight folding of leucosomes with axial plane parallel to the main foliation (Fig. 6B). Quartz veins are present as parallel to the foliation (Fig. 6B), but part of the quartz veins occur also as cross-cutting features in which the veins are folded with axial plane parallel to the main foliation. The presence of quartz veins along the shear fabrics (Fig. 6B and 7A) is indicative of pronounced fluid flow associated with the shearing processes. Within the mineralised zone part of the quartz veins are arsenopyrite bearing (Fig. 6C). The lithology within Välimäki and its vicinity consists of paragneisses (Fig. 6A) with both pelitic and psammitic compositions and stromatic textures as a common feature. Garnet porphyroblasts are very common as a layer-bound or a pervasive feature in

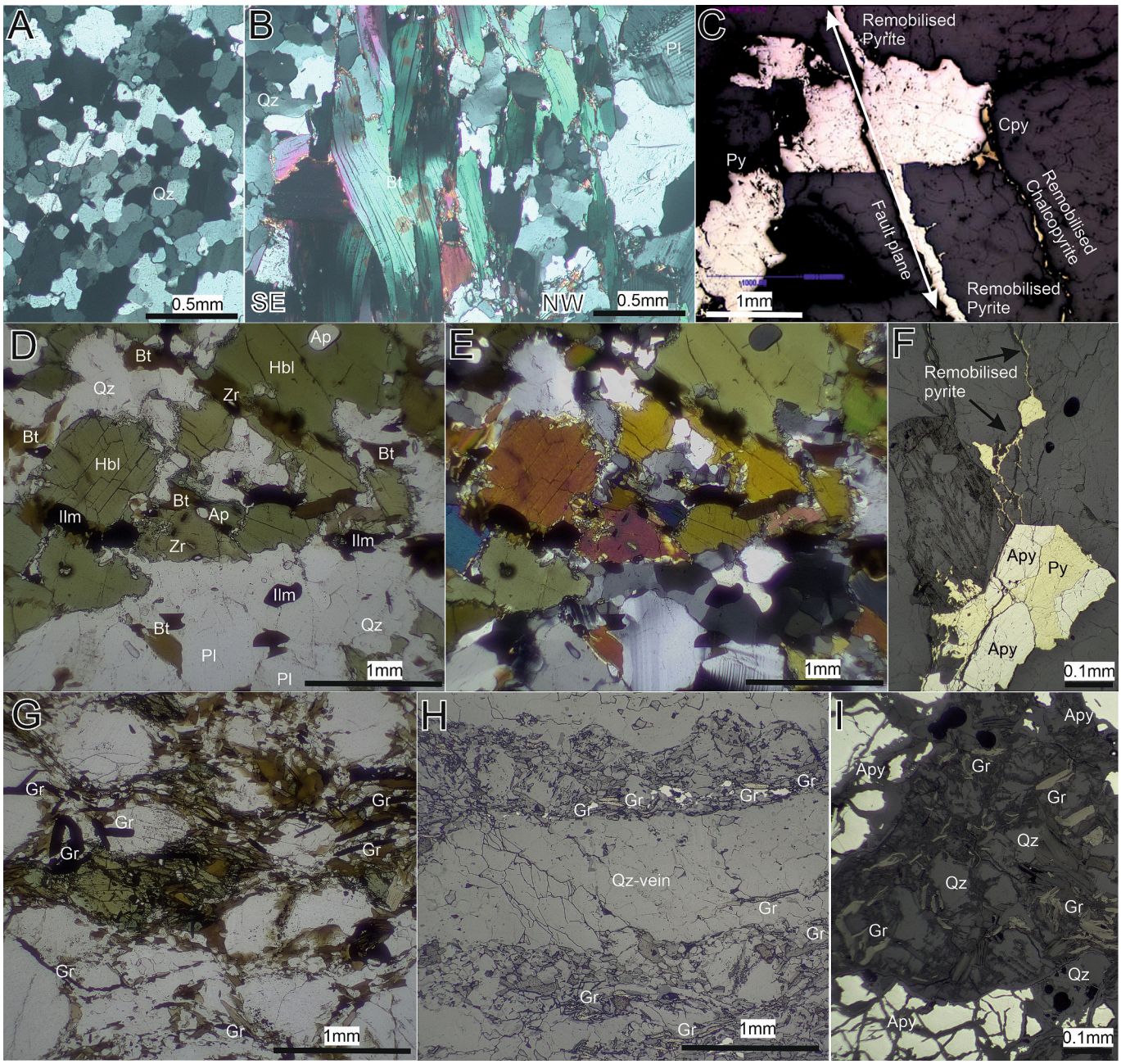

Fig. 7. Photomicrographs of Välimäki and Kultakallio. A. Static recrystallization of quartz from Välimäki. B. Crenulation folding visible in the biotite grains, quartz grains display static recrystallization. View towards SW. C. Typical ore minerals of Välimäki and remobilisation of sulphides along a fault plane, reflected light (photo adapted and modified after Kärkkäinen et al., 2012). D. Unaltered Kultakallio gabbro (JKKA-2022–1.1) in plane polarised light, E. cross-polarised light. F. Typical ore minerals of Kultakallio (JKKA-2022–1.4) and remobilisation of sulphides, reflected light. G. Slice of sheared and graphite bearing gabbro (JKKA-2022–1.2) within quartz vein in plane polarised light, H. Graphite flakes bordering quartz vein in Kultakallio (JKKA-2022–1.2), reflected light. I. Strongly silicified Kultakallio gabbro within a shear zone with graphite and broken arsenopyrite (JKKA-2022–1.5), reflected light. Qz = quartz, Bt = biotite, Pl = plagioclase, Hbl = hornblende, Ilm = ilmenite, Ap = apatite, Gr = graphite, Py = pyrite, Cpy = chalcopyrite, Apy = arsenopyrite.

the Välimäki prospect, the latter indicating hydrothermal alteration in the area.

4.2.2. *Kultakallio*

The Kultakallio area is significantly more restricted in the number of outcrops with respect to Välimäki. Three foliation measurements show mutually sub-parallel attitudes with moderate dips towards the SSE, and one lineation measurement taken from the gabbro intrusion has a sub-horizontal SW plunge (Fig. 6D). One strike-slip type shear zone with parallel quartz and sulphide veins was observed in the gabbro outcrop.

Mineralogically, the gabbro can be classified as hornblende gabbro and it consists of plagioclase (labradorite-andesine), hornblende (primary and secondary), biotite (secondary), quartz (mostly secondary), garnet (almandine; secondary) and varying amounts of ilmenite, apatite, sulphides and graphite (Fig. 6E, 7C-F). In places quartz is abundant due to later silicification and quartz veining of the rock. Garnets are present in large amounts, indicating strong hydrothermal alteration in the area. Two generations of quartz veins are present in the gabbro: i) veins of the older generation are 5–10 mm in thickness, they occur parallel with the foliation and are locally folded, ii) veins of the younger generation (10–150 mm thick) are sub-vertical and trend NNW, hence sharply crosscutting the main fabric of the gabbro (Fig. 6E). Gold occurs in both

types of quartz veins (Kärkkäinen et al., 2016). Sulphides are present as disseminations in gabbro and paragneiss, whereas the high-grade intersections of gold occur nearly exclusively within the gabbro. Graphite is an abundant phase within the sheared and altered parts of the gabbro (Fig. 7E and F).

4.3. U-Pb age data

4.3.1. Välimäki

Zircon

Zircons and monazites were separated from the Välimäki foliation-parallel granitic leucosome veins, which represent partial melts of the local paragneisses. The shapes of the zircon grains vary from elongated, doubly-terminated to stubby, equant crystals shapes (Fig. 8A). Many of the grains are subrounded and their typical lengths are 100–200 μm with few grains exceeding lengths of 250 μm. Grain widths ranges between 50–100 μm. Most of the grains are metamict to some degree and this alongside fracturing was the dominant decisive factor for selecting suitable grains for the U-Pb analysis. Detrital cores are present in multiple grains as well as BSE-dark inclusions.

In all, 43 spots were analysed on 35 grains and two main age populations were found. The most homogeneous population is defined by 16 analyses on rims and homogeneous grains/domains (Fig. 8A), and these show a concordia age of 1887 ± 4 Ma (n = 15, MSWD = 0.0085) and an almost identical weighted average $^{207}Pb/^{206}Pb$ age of 1887 ± 4 Ma (n = 16, MSWD = 0.44; Fig. 9A and B). This population shows very low Th/U ratios between 0.002 and 0.053. The second population consists of analyses on cores and heterogeneous grains and these yielded $^{207}Pb/^{206}Pb$ ages between 2858 and 1899 Ma. These are considered as inherited. Th/U ratios are variable for these analyses ranging from very low values of 0.003 to 1.178 with an average value of 0.232. Also, three younger ages are found showing $^{207}Pb/^{206}Pb$ ages between 1873 and 1864 Ma. The spots of these analyses are located on similar domains as for the first group. These analyses show low Th/U ratios around 0.004.

Monazite

The monazite grains were separated from the same leucosome sample as the zircons. The diameters of the rounded grains range between 100–350 μm (Fig. 10B). The internal texture is rather homogeneous, but a faint growth zoning is present revealing possible core-rim relations and irregular zonation patterns can be detected by the subtle change of brightness on the BSE images. Fracturing is present but not as commonly as in the zircon grains. Unknown inclusions can be found in several grains, but on average the monazites are homogenous.

In all, 23 spots were analysed on 19 grains. The results are quite homogenous, but two age populations are possible to detect without a clear textural association. The older population is defined by eight analyses which yield a concordia age of 1816 ± 8 Ma (n = 4, MSWD = 0.0105) and slightly younger weighted average $^{207}Pb/^{206}Pb$ age of 1813 ± 7 Ma (n = 8, MSWD = 0.19; Fig. 9C and D). These analyses occur usually in grain interiors. The younger population consists of 15 analyses, and they show a concordia age of 1794 ± 4 Ma (n = 12, MSWD = 0.096) and a similar weighted average $^{207}Pb/^{206}Pb$ age of 1794 ± 5 Ma (n = 15, MSWD = 0.091). The younger ages are usually from the rim part of the grains, but young cores/inner parts are also present. Using all the analyses, it is not possible to calculate a concordia age but a weighted average $^{207}Pb/^{206}Pb$ yields an age of 1801 ± 4 Ma.

4.3.2. Kultakallio

Five thin sections were prepared for *in-situ* age determinations from the Kultakallio gabbro: an unaltered gabbro (JKKA-2022–1.1), an intersection between an older generation sub-conforming quartz vein and a younger cross-cutting quartz vein with surrounding gabbro (JKKA-2022–1.2), a garnet-bearing altered gabbro (JKKA-2022–1.3), an arsenopyrite-bearing gabbro (JKKA-2022–1.4) and a sheared arsenopyrite-bearing gabbro (JKKA-2022–1.5).

Zircon

The zircons from the gabbro are quite evenly distributed on the thin sections. The only exception is the sample from a quartz vein in the gabbro (sample 1.2) in which the zircons only occur in the gabbro. The zircon grains are mostly elongated with lengths between 15 and 200 μm. The textures vary from euhedral to anhedral with a majority showing slightly rounded subhedral morphology. The grains occur as inclusions and on the borders of other minerals. The BSE scans reveal possible cores and rims and faint oscillatory zonation on the grains but otherwise the grains are seemingly homogeneous. All the samples provided similar zircon U-Pb results and therefore the results are combined and addressed together.

In all, 112 analyses were conducted on 108 grains and four age populations can be identified. No explicit pattern of ages based on zircon texture or mineralogical association were detected. Therefore, the division into the age population is based on the age data and Th/U ratios only. The largest population shows a concordia age of 1884 ± 3 Ma (n = 35, MSWD = 0.41) and a weighted average $^{207}Pb/^{206}Pb$ age of 1885 ± 4 Ma (n = 44, MSWD = 0.098; Fig. 9E and F). Th/U ratios vary between 0.1 and 0.54 with an average value of 0.33. The younger population shows a concordia age of 1856 ± 5 Ma (n = 24, MSWD = 1.05) and a slightly older weighted average $^{207}Pb/^{206}Pb$ age of 1859 ± 5 Ma (n = 37, MSWD = 0.099). The average Th/U ratio for this population is 0.22. The youngest population shows a range of $^{207}Pb/^{206}Pb$ ages between 1840 and 1799 Ma with a gradual decrease in ages from 1840 Ma to 1813 Ma and a flattening trend at younger ages. A weighted average $^{207}Pb/^{206}Pb$ age of 1808 ± 6 Ma (n = 18, MSWD = 0.26) was calculated for the ages between 1799 and 1813 Ma. Alternatively, a weighted average $^{207}Pb/^{206}Pb$ age of 1815 ± 5 Ma can be calculated for the whole

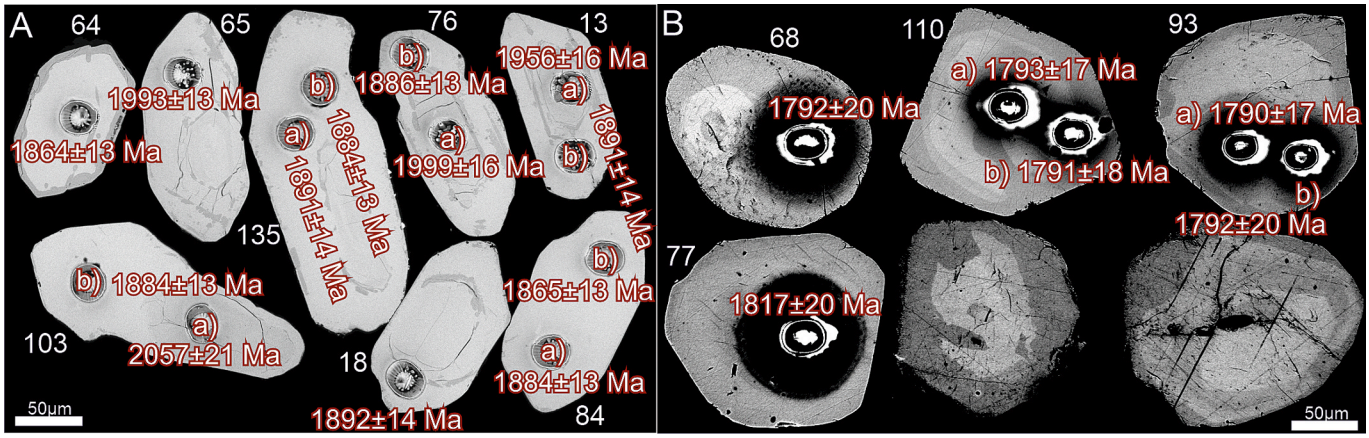

Fig. 8. Characteristic zircon (A) and monazite (B) BSE-images from Välimäki with $^{207}Pb/^{206}Pb$ spot ages.

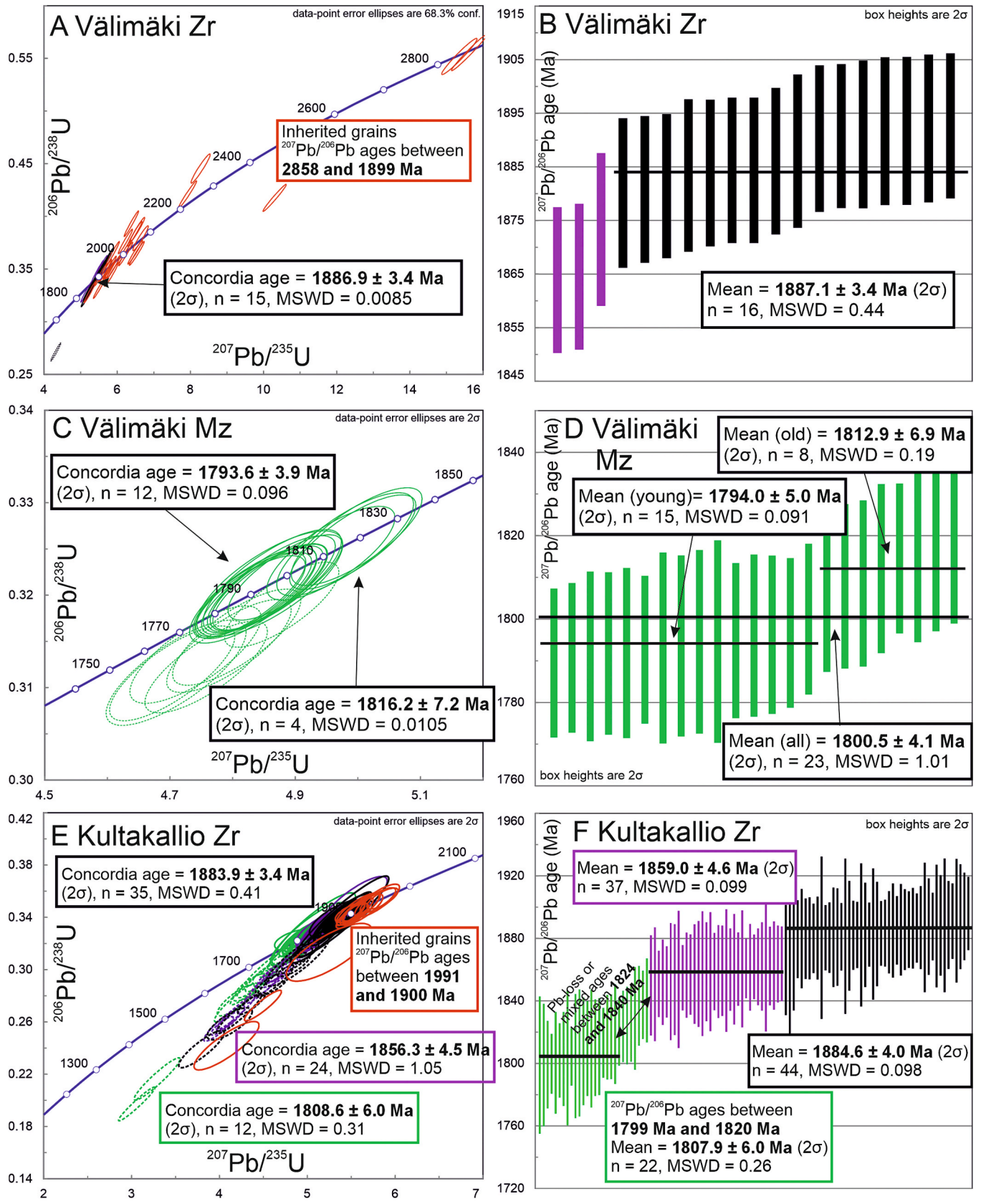

Fig. 9. U-Pb data for the analysed zircons and monazites from Välimäki and Kultakallio. Red colour indicates inherited grain/domain, black colour crystallisation from melt, purple metamorphic crystallisation and green hydrothermal origin. The dashed error ellipsoids represent analyses omitted from the concordia age calculation due to discordancy. Analyses interpreted as inherited are not shown in $^{207}Pb/^{206}Pb$ diagrams. Zr = zircon, Mz = monazite. All the U-Pb results, and the Th/U ratios are provided in Electronic Appendix B. (For interpretation of the references to colour in this figure legend, the reader is referred to the web version of this article.)

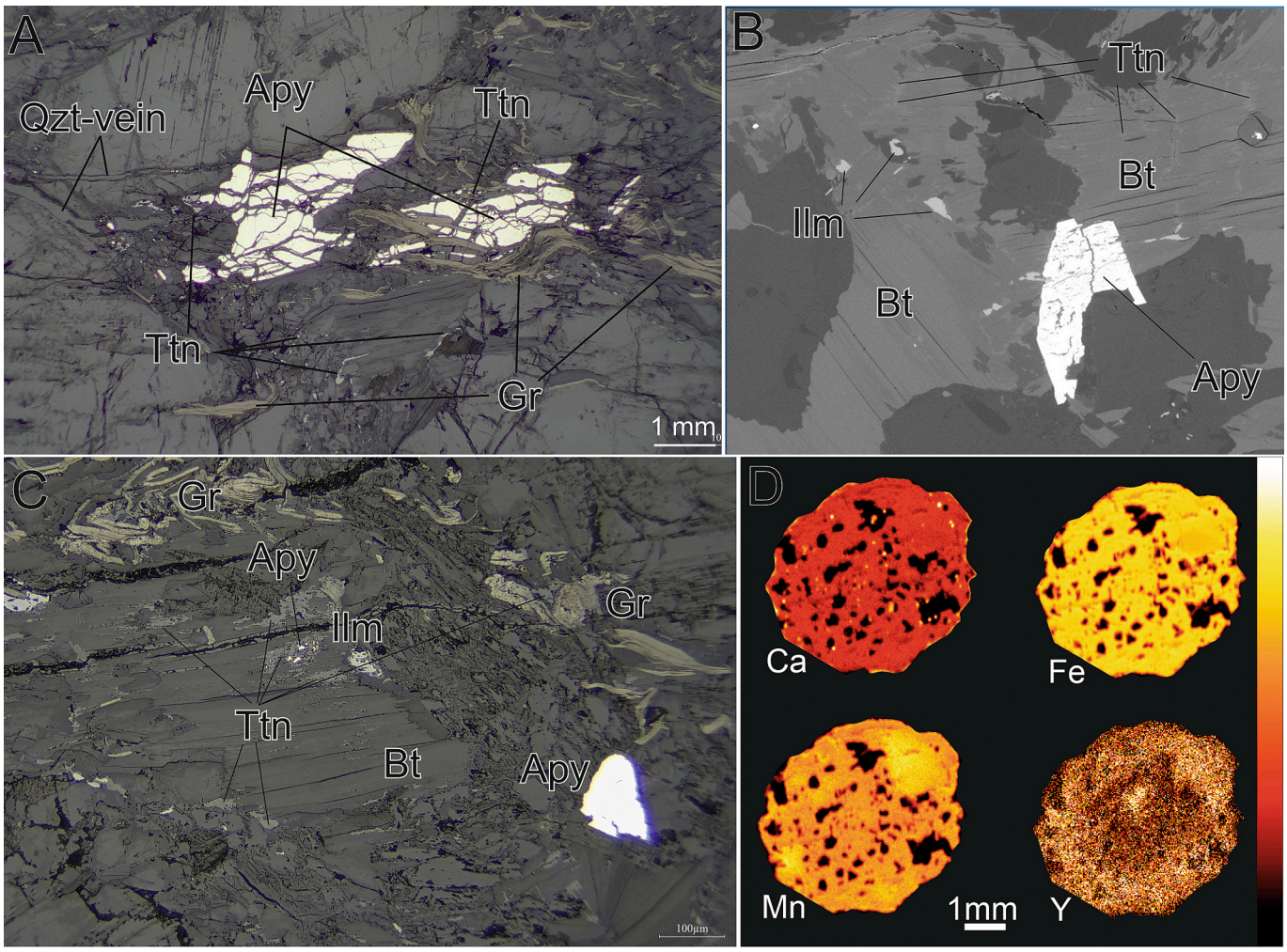

Fig. 10. A. Breakdown of a gold-bearing arsenopyrite during CO2-rich fluid pulse indicated by quartz veins and graphite penetrating into cracks in arsenopyrite. Titanites are associated with graphite and occur in contact with sulphide and graphite (reflected light; JKKA-2022–1.5). B. BSE-image of the exsolution type titanites (JKKA-2022–1.5). C. Titanite replacing arsenopyrite in centre of the figure (reflected light; JKKA-2022–1.5). D. µXRF elemental maps of the dated garnet (µXRF analysis made from the counterpart of the thin section; JKKA-2022–1.3). The mapped element is labelled in the bottom left corner. The maps show relative concentrations and are illustrated with lighter colours corresponding to high concentrations and darker colours corresponding to lower concentrations. Apy = arsenopyrite, Ttn = titanite, Qzt = Quartz, Bt = biotite, Ilm = ilmenite, Gr = graphite.

population. Majority of the spots in the youngest group are located on the zircon rims and this population shows the lowest Th/U ratios with an average value of 0.11. The oldest population consists of presumably inherited grains and domains yielding $^{207}Pb/^{206}Pb$ ages between 1991 and 1900 Ma.

Titanite and garnet

Titanites are common in the sheared, altered and sulphide-bearing Kultakallio samples JKKA-2022–1.4 and 1.5 but they were not detected from the least altered samples JKKA-2022–1.1 and 1.2. Two types of titanites were observed: i) exsolution intergrowth in biotite (Fig. 10B), which are interpreted to represent the by-product of chloritisation of Ti-bearing biotite (Janeczek, 1994) and ii) anhedral, roundish grains in contact with and near sulphides, ilmenites and graphite flakes (Fig. 10A). Several titanites were analysed of both populations. However, the intergrowths were too thin for proper dating by LA-ICP-MS.

The garnets in Kultakallio show variable sizes between 0.5 to 7 mm. They are subhedral and usually rounded to subrounded. The garnets have numerous inclusions including zircon, ilmenite, pyrrhotite, biotite, plagioclase and quartz. Due to abundant inclusions the garnets show spongy textures resembling those of the hydrothermal origin (e.g., Sun et al., 2020). One garnet grain was selected for U-Pb dating. The mapped garnet shows no elemental zonation except for Y, which shows a high Y core, lower Y mantle and high Y outer rim (Fig. 10D).

In all, 45 spots were analysed on the titanites of sample JKKA-2022–1.5. Twenty-eight analyses yield a lower intercept age of 1786 ± 58 Ma (MSWD = 4.1) in the Tera-Wasserburg diagram with data-defined initial common $^{207}Pb/^{206}Pb$ composition of 0.865 (Fig. 11A). Titanites representing the exsolution of biotite were too thin for laser ablation and thus these analyses are scattered around the diagram (grey ellipses) and were omitted from age calculations.

Eight spots, placed on the outer rim, were analysed on a single garnet grain of sample JKKA-2022–1.3. These yield a lower intercept age of 1809 ± 470 Ma (MSWD = 0.0078) in the Tera-Wasserburg diagram with data-defined initial common $^{207}Pb/^{206}Pb$ composition of 0.85 (Fig. 11B). Large errors are due to low U content of the garnet and small number of analyses.

5. Discussion

5.1. Age constraints

We suggest that the zircon U-Pb age of 1887 ± 3 Ma shown by the low Th/U zircon rims and homogeneous domains from the Välimäki leucosome represents the age of the melt-bearing phase, which can be

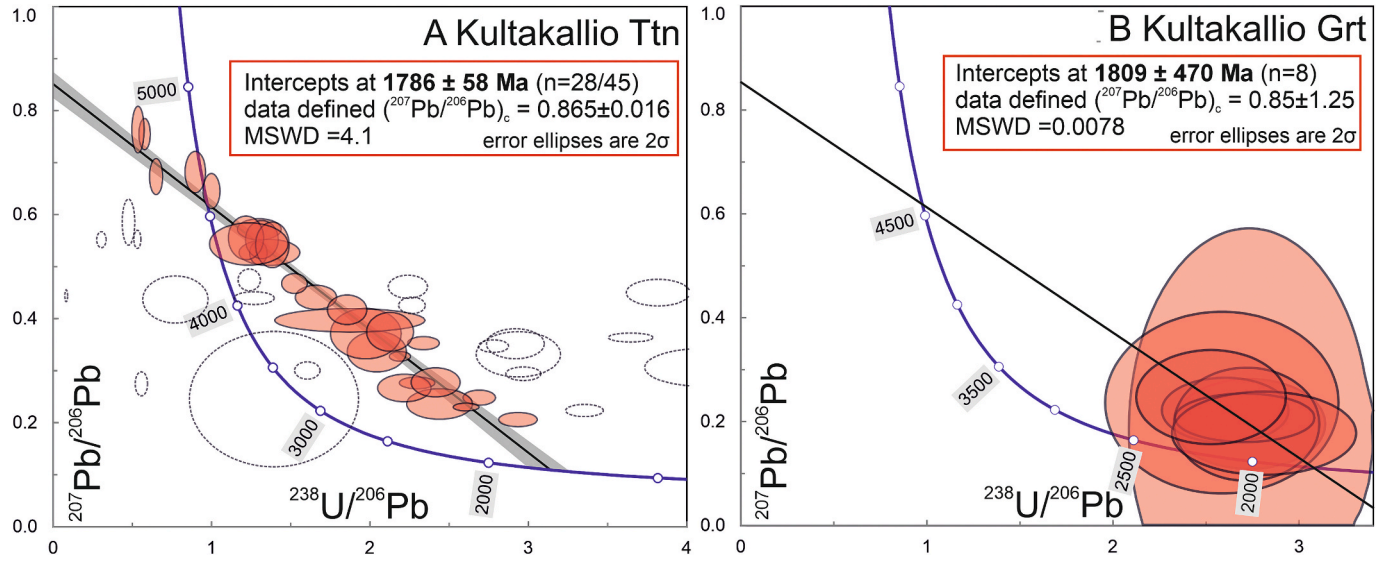

Fig. 11. A. Tera-Wasserburg concordia diagrams for the Kultakallio titanites (A) and garnet (B). Isochrons and pooled lower intercept ages are shown as calculated in Isoplot 4.15 (Ludwig, 2012). The data are uncorrected for common Pb (see Electronic Appendix A). The analyses illustrated with dashed ellipses were omitted from the calculation.

correlated to the age of the first metamorphic event (M1) in the area. This is in line with previous studies dating the peak metamorphism in the Pirkanmaa belt at ca. 1.88 Ga (Mouri et al., 1999; Rutland et al., 2004; Lahtinen et al., 2009) and in the Vaasa migmatitic complex situated north of the study area (Chopin et al., 2020). Two younger metamorphic events at ~ 1.86 Ga and ~ 1.83 Ga have been identified within the Olkiluoto domain located about 50 km west from the Kullaa area (Fig. 1) by zircon U-Pb (1.86 Ga; Mänttäri et al., 2006; Engström et al., 2022) and garnet Lu-Hf ages (1.83 Ga; Engström et al., 2025). Based on the above ages, Engström et al., (2022, 2025) correlated the Olkiluoto area to the Häme belt and Ljusdal domain in Central Sweden (Fig. 1A) rather than to the Pirkanmaa belt. This is supported by the result of this investigation, highlighting the difference between the Häme and Pirkanmaa belts and the distinct metamorphic evolution of the two belts.

A crystallisation age of 1885 ± 4 Ma is suggested for the Kultakallio gabbro. This is supported by several details: i) 1885 Ma population is the largest and most homogenous age group, ii) the 1885 Ma age group shows the highest Th/U ratios, although they are rather low in general, which probably reflects coeval precipitation of apatite (Fig. 7C), iii) 1885 Ma can be linked to the major 1.89–1.87 Ga magmatic event in southern Finland (e.g., Suominen, 1988; Kähkönen, 2005; Saalmann et al., 2010; Tiainen et al., 2013; Kara et al., 2020) and iv) the gabbro shows similar foliation patterns compared to the surrounding supracrustal rocks supporting pre to syntectonic crystallisation. The 1885 Ma age is also similar to the 1884 ± 4 Ma quartz diorite, the host rock of the Jokisivu gold deposit in the Häme belt (Saalmann et al., 2010; Fig. 1B). Moreover, similar ages have been obtained for numerous other mafic plutonic mafic rocks showing continental arc affinities from SW Finland (e.g., Kähkönen, 2005; Kara et al., 2018, 2020).

The ca. 1860 Ma zircon population in Kultakallio can be interpreted in two ways: (i) the age represents an independent geological event or (ii) the population is a mixed age between the crystallisation and the young population (see discussion below). We prefer the first alternative since the age data are homogeneous and well-constrained (Fig. 9F). Moreover, there is growing evidence of metamorphism at ca. 1.86 Ga in southern Finland (Väisänen et al., 2021; Vehkamäki et al., 2021; Engström et al., 2022) and in central Sweden (Hermansson et al., 2007; 2008; Högdahl et al., 2012). The extent or conditions of this metamorphic event are not well established, but Kara et al. (2021) speculated that the driver for the metamorphism was crustal extension combined with arclogite delamination (Kara et al., 2020), which led to upwelling of the upper mantle and increasing heat flux from the mantle to the crust. Evidence for the mantle derived magmatism in southern Finland (e.g., Väisänen et al., 2012; Kara et al., 2020; Johnson et al., 2024) as well as an extensional tectonic regime during this period (Bergman et al., 2008; Lahtinen and Nironen, 2010) is robust so we suggest that the ca. 1860 Ma zircon population represents a secondary metamorphic event (M2) in the area. This thermal event is not that prominent in the Välimäki zircon data but there are three analyses showing ^{207}Pb/^{206}Pb ages between 1873 and 1864 Ma, which can be interpreted as belonging to this event.

The monazites from the Välimäki area appear as clusters in the thin sections, which is strong evidence of hydrothermal origin (Schandl and Gorton, 2004). The monazites reveal two age populations at 1813 ± 7 Ma and 1794 ± 5 Ma. Although some uncertainty remains in subdivision of the age data into two populations, we consider this option interesting and plausible as several fluid pulses are known to have occurred within the area as indicated by the presence of several quartz vein populations. Moreover, the enhanced BSE-images taken after the monazite dating reveal concentric zonation in many grains (Fig. 8B), which might suggest two-stage precipitation of monazites in 1813 and 1794 Ma. This is in line with the titanite U-Pb data showing the age of 1786 ± 58 Ma being the youngest age of all the dated minerals. The large error reflects the heterogeneity of the titanites but also their synchronous precipitation with hydrothermal fluid activity and their replacement of ilmenite and arsenopyrite. Thus, they are expected to represent late hydrothermal activity within the study area.

The youngest zircon population in Kultakallio is very similar to the monazite age in Välimäki and the zircon age of 1808 ± 6 Ma overlaps within errors the older monazite age of 1813 ± 7 Ma. The age and low Th/U ratio of 0.11 suggest hydrothermal origin for these zircon domains (e.g., Hoskin, 2005; Zhai et al., 2022) or alteration and re-equilibration by hydrothermal fluids (e.g., Geisler et al., 2007; Park et al., 2016). The garnet U-Pb age of 1809 ± 470 Ma shows huge errors due to the low U content making the age imprecise. However, the face value age of 1809 Ma is reasonable and agrees with the young zircon and monazite ages. The spongy texture, multiple inclusions and homogenous elemental distribution support the hydrothermal origin for the garnets (e.g., Sun et al., 2020). This suggests that the garnets are related to hydrothermal alteration of the gabbro during fluid activity at 1.8 Ga. The titanite ages are roughly similar and the younger monazite populations are similar within error to the apatite U-Pb and Lu-Hf ages of 1778 ± 16 Ma and

1782 ± 19 Ma, respectively, obtained from Olkiluoto area (Engström et al., 2025). The four dated apatite grains occurred as inclusions in garnet rims and were classified as metamorphic. Based on the locking temperatures of Lu-Hf and U-Pb systems this would indicate temperatures over 650 °C (Glorie et al., 2024; Chew and Spikings, 2021) at 1.78 Ga, which is in conflict with our results. We prefer an alternative interpretation, also addressed by Engström et al. (2025), that the apatites are metamorphic but isotopes systems were reset during hydrothermal activity.

During partial melting and subsequent crystallisation, zircons precipitated, and zircon rims grew on detrital cores which were preserved up to the temperatures of 750–800 ℃. The 1887 Ma zircons are therefore formed during partial melting and melt crystallisation, a feature absent in the 1.86 and 1.80 Ga events in the study area. The monazite ages are prominently 80 Myr younger than the zircon ages in Välimäki. This could be attributed to the lower closure temperature of the monazite (e.g., Parrish, 1990; Cherniak and Watson 2001; Cherniak et al., 2004) or lower preferred growth temperature (Kelsey et al., 2008). However, many studies have remarked the reactiveness of monazites to changing conditions in fluid-rich environment as well as complexity of monazite growth and (re-)precipitation processes (e.g., Hermann and Rubatto 2003; Fitzsimons et al., 2005; Högdahl et al., 2012; Mottram and Cottle, 2024). Therefore, an alternative explanation is addressed. An age difference this big suggests that the monazites were not crystallised during the metamorphic peak at 1887 Ma or the monazites were precipitated but they were completely reset afterwards. The U-Pb-Th compositions in all the monazite analyses are very similar, suggesting that none of them were grown during the 1887 Ma metamorphism and they are related to the hydrothermal activity at ca. 1.80 Ga. On the contrary, the zircon grains in Välimäki display no 1.80 Ga ages, indicating that the hydrothermal event at 1.80 Ga was not strong enough to overprint the zircon grains. Thin rims can be detected on the Välimäki zircons, but their age remains unknown. Similar results during metamorphism and subsequent hydrothermal activity have been recognised in the Ljusdal Domain in central Sweden by Högdahl et al. (2012) where zircon yielded 1.87–1.86 Ga ages and monazites displayed double peaks at 1.87–1.86 and 1.82–1.80 Ga. The formation of the monazite in the Ljusdal Domain was also correlated to subsolidus conditions and late-orogenic, shear zone –controlled, hydrothermal activity (Högdahl et al., 2012). In addition, fluid activity and fluid composition can greatly affect zircon precipitation (e.g., Park et al., 2016) and zircon formation in temperatures as low as 300° C have been detected (Zhai et al., 2022), which can explain the post 1.88 Ga zircon occurrence in Kultakallio. The occurrence of hydrothermal garnet and graphite in Kultakallio could indicate a stronger hydrothermal activity or different fluid composition in Kultakallio and thus explain the (re-)crystallisation of zircon at 1.80 Ga.

In all, we suggest that the 1.885 Ga event represents the peak metamorphism, partial melting and magmatism, the 1.86 Ga event represents a secondary metamorphism whereas the 1.81–1.78 Ga events comprise merely hydrothermal activities in the study area.

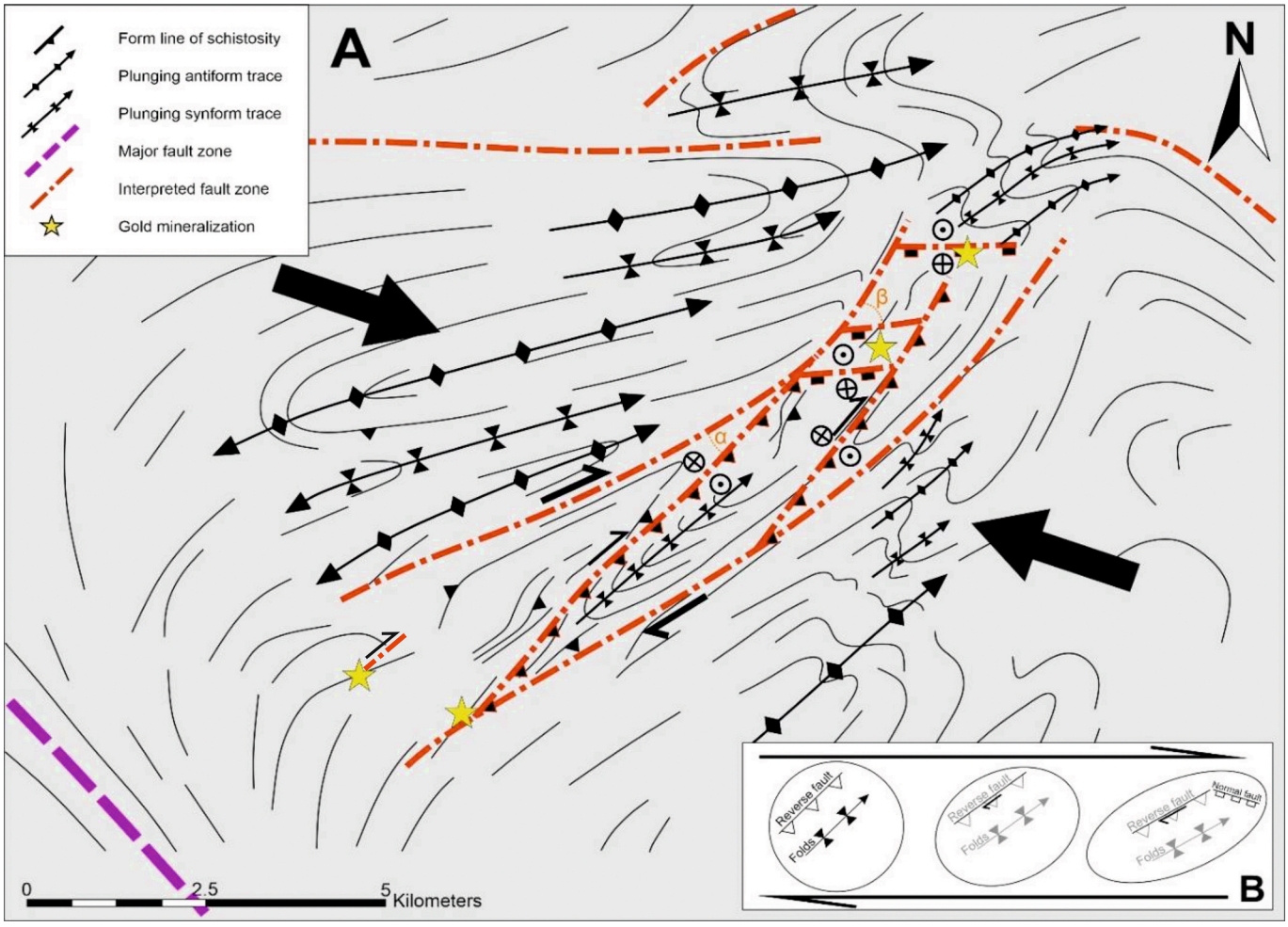

Fig. 12. A. A simplified form line map of the study area hosting the high strain structures. Arrows denote WNW-ESE shortening direction at 1.83–1.80 Ga. B. Strain ellipse depicting the progressive deformation and formation of structures.

5.2. Structural evolution

Melt-formation was either synchronous or pre-dates the first major deformation event (D2) responsible for the map-scale folding, as suggested by the presence of both foliation-parallel (Fig. 6B) and folded leucosomes (Fig. 5A and 6B). Thus, generation of high-strain zones (reverse faults/thrusts) along the axial surfaces (Fig. 12A and B) are interpreted to have formed synchronously with melt-formation. For these reasons, the mapped NE trending dextral high-strain zone(s) are likely 1.89–1.88 Ga in origin, with later reactivation(s) that are responsible for the mineralisation. The proposed timing of the folds with (E)NE-(W)SW trending axial surfaces correlates with the regional 1.88 Ga D2 event (Saalmann et al., 2009, 2010; Lahtinen et al., 2023). The general NE-SW structural trend suggests NW-SE principal stress orientation during the D2 event, taken that the bounding NNW-trending KySZ did not contribute to strain localisation at 1.88 Ga. The later, post-D2 timing of the KySZ is supported by the distinct sinistral deflection of the planar and linear fabrics within the Pomarkku block into the KySZ trend (Figs. 2-4). Pajunen et al. (2008) suggest that the Pomarkku block underwent clockwise rotation during the NW-SE transpressional event, supported by the left-lateral kinematics of the KySZ and oblique dextral kinematics of the KaSZ. The clockwise rotation of the Pomarkku block is a viable explanation for the formation of semi-crustal-scale apparent right-lateral features in the NE-trending gold critical zone (Fig. 12A), acting as a hinge-zone between two separate, mechanically rigid plutonic units to the north NW and SE.

North of the present study area, Lahtinen et al. (2014; 2023) suggested that a NW-SE principal stress orientation at 1.875 and 1.865 Ga was responsible for buckling of a pre-existing linear orogenic belt, and subsequent formation of the coupled Bothnian oroclines. The above model of buckling is in concert with the NW-SE main shortening direction along the KySZ (Reimers et al., 2018). Furthermore, the interpreted SW-directed flow of the Central Finland Granitoid Complex during the buckling of the orogen is a plausible interpretation for the thrust-type kinematics observed along the KaSZ, which occurs along the eastern margin of the Pomarkku Block. Thus, a NW-SE −oriented stress regime would be suitable not only to the formation of the NE-SW −oriented structures during D2, but also the formation of the KySZ and KaSZ during the $D_{OROCLINE}$ event. This suggests a prolonged or pulsating NW-SE-oriented stress regime during 1.89–1.865 Ga.

An extensional period between 1.865 and ~ 1.84 is widely recognised in SW Finland and Central Sweden (Bergman et al., 2008; Lahtinen and Nironen, 2010). Clear extensional features were not identified except the normal faulting interpreted between subparallel strike-slip and oblique-slip zones (Fig. 12A). Therefore, if present, the strain is suggested to localise into pre-existing structures during extensional events.

WNW-ESE is identified as the crude shortening direction, which is suggested to have occurred partly during the later deformation event (D3) based on progressive deformation (Fig. 12B), reactivation and bending of the pre-existing NE-SW oriented structures (Fig. 12A). This is correlated with the regional D6 (Saalmann et al., 2009) or D4 (Lahtinen et al., 2023) event between 1.83 and 1.78 Ga. During the metamorphic event (M1), strain was distributed evenly throughout the study area due to higher T whereas strain was localised into narrow shear zones in the younger deformation event. The contrasting mechanical behaviour of this zone is most likely the consequence of the high proportion of the supracrustal units within the host-rocks (Fig. 2) and their more ductile flow with respect to the more rigid plutonic units, abundant in the northern parts of the study area, or the presence of a pre-existing structure underlying the gold-bearing high-strain zone at depth. D3 is not suggested to be a homogeneous deformation event lasting 50 Myr but rather a series of shorter contractional intervals wherein stress remained WNW-ESE directed.

Reimers et al. (2018) reported that the NW-SE striking KySZ displays a later brittle deformation overprint in an E-W compressional setting with east-block-up −kinematics. Observations of several conjugate fracture sets conforming to this E-W compressional regime were made in this investigation, congruent with the study by Reimers et al. (2018). These structures represent the latest notable deformation event within the study area. The age of the brittle deformation is unknown but motion along these brittle structures was not recognised, and these fractures are dominantly vacant of mineral fillings, an indicator of absence of volatiles during this event. The NW-SE oriented planar structures in the KySZ have most likely hosted the majority of movement due to their more favourable orientation with respect to the E-W oriented compressional regime.

5.3. Gold-critical structures and the age of the fluid activity

The KySZ and KaSZ very likely played a major role in fluid flow acting as fluid conduits for auriferous fluids from depth and as first order structures (Fig. 3) whereas the NE-SW oriented strike- and oblique-slip structures (Fig. 12A) form the second order structural setting. The Välimäki deposit is located within the area of influence of the dextral second-order strike-slip structures. The drill-core data show the presence of gold-critical vein arrays in narrow shear zones and as a foliation-parallel feature (Kärkkäinen et al., 2012). The shear-related veining most likely branches, forming the third order structures, from the strike-slip zone hosting both antithetic and synthetic kinematics and related orientations. In Kultakallio, the weak fold pattern visible in the geophysical data suggests that the prospect is sited at the fold hinge (Fig. 4). Drill hole data indicated parallel shearing, both mylonitic and breccia-type, with the foliation (Kärkkäinen et al., 2016). These structures indicate reactivation of pre-existing structures during the 1.83–1.78 Ga WNW-ESE transpressional regime and provided fluid conduits for the mineralisation. The competence contrast between the rigid Kultakallio gabbro and adjacent paragneiss units is interpreted to be liable for the formation of gold-bearing structures even though larger scale structures, present in other prospects, are mostly absent.

Quartz veining is interpreted to be the gold-critical structure in Välimäki and Kultakallio and these are sited in at least three distinguishable settings/events: i) foliation-parallel, ii) younger, foliation-intersecting and −parallel and iii) shear-related and crosscutting veining. The first and third groups have rather well constrained structural setting and timing, but the second group were emplaced during a wider time interval. The foliation-parallel veining is generally associated with partial melting and leucosome veins (Fig. 6B) and interpreted to be the oldest generation of veining, representing *syn*-tectonic emplacement during or slightly after the peak metamorphism at 1887 Ma. Folding of these veins with axial planes parallel to the main foliation supports the syntectonic formation environment (Fig. 6B). The quartz veins intersecting the dominant foliation but folded with axial planes parallel to the main foliation are also present, indicating syn- to post-tectonic emplacement. The first generation veins are abundant in Välimäki but are not detected within Kultakallio gabbro although present in the surrounding paragneiss.

The second group is the least well-defined of the vein generations and includes also quartz veins that have intruded along the foliation but are younger than the first group of veins (Kärkkäinen et al., 2016). The width of the veins varies between a few millimetres to two centimetres. In Välimäki these occur as swarms of thin veins or are hosted by narrow foliation parallel shears (Kärkkäinen et al., 2012) whereas in Kultakallio these have brownish ("rusty") tint, and they appear as foliation-parallel or gently intersecting clusters (Kärkkäinen et al., 2016). Thus, their distinction from the first generation veins can be ambiguous, however, in both locations the second group veins contain arsenopyrite (Fig. 6C and E; Kärkkäinen et al., 2012; 2016). Based on our young zircon, garnet and older monazite ages of ca. 1810 Ma we suggest that this occurred in 1815–1805 Ma and is related to the D3 event at 1.83–1.78 Ga (D4: Lahtinen et al., 2023; D6: Saalmann et al., 2009). Saalmann et al. (2010) correlates this to WNW-ESE dextral transpression, supporting our

interpretation. Moreover, the timing is in line with ages obtained from the Jokisivu gold mine. Saalmann et al., (2010) reported an age of 1802 ± 15 Ma from the low Th/U zircon rims from the quartz diorite host rock and a similar 1801 ± 18 Ma titanite age from the ore zone. Additionally, a cutting pegmatite dyke yielded a zircon age of 1807 ± 3 Ma and a monazite TIMS age of 1791 ± 2 Ma from the same location, which were regarded as the minimum age for the mineralisation.

The third generation of quartz veins contains shear-related veins that crosscut the foliation and veins systematically oriented at NW-SE with steep dips, displaying no folding patterns and crosscutting the older sets of quartz veins. The NW-SE −oriented veins are not hosted by shear zones and display linear shapes and are generally thinner, except in Kultakallio (Fig. 6E), than the older vein generations. The geometries and characteristics of this vein array support the formation above or within the brittle-ductile −transition zone. Shear zones host quartz veins in multiple orientations, e.g. N-S- and E-W −oriented antithetic sinistral veins and are most likely related to the same event as the foliation intersecting veins. Therefore, the stress regime is somewhat suitable for both (i) the WNW-ESE transpressional D3 event at 1.83–1.78 Ga or (ii) with the E-W compressional paleostress orientation during the brittle deformation of the KySZ (unknown age; Reimers et al., 2018). The orientation and relative timing are similar to those at the Satulinmäki deposit where slightly older NE-SW trending shear zones are cut by NW-SE trending faults (Saalmann et al., 2009). Based on this, and the supposedly volatile-free conditions during the brittle deformation we prefer the first alternative. We suggest that the younger ca. 1795 Ma monazite population and the titanite age of 1786 Ma represent the age frames of this quartz vein set. This means they belong to the D3 event within a WNW-ESE transpressional setting but the conditions reached the ductile–brittle boundary approximately at 1.80 Ga. Moreover, the relevance of NW-SE −oriented faults are identified also in Jokisivu (Saalmann et al., 2010) and Uunimäki deposits (Kara et al., 2021).

The age of magmatism and metamorphic peak at 1887 Ma naturally defines the maximum age for mineralisations not just at Kultakallio and Välimäki, but also in the whole Kullaa area. Temperature within the crust is suspected to remain above 600 °C until 1840–1830 Ma due to a secondary metamorphic peak at 1860 Ma (Fig. 13) inhibiting the precipitation of sulphides and gold (Tomkins et al., 2006). The occurrence of arsenopyrite is restricted to altered zones, quartz and sulphide veins and shears suggesting an exclusively hydrothermal origin. Although the As-Au system can be linked to crustal depths over 12 km and thus rather high temperatures (Groves et al., 2020), precipitation of arsenopyrite (or gold) does not generally occur above 550 °C at 5kbar (Sharp et al., 1985; Pokrovski et al., 2002; Groves et al., 2020). Therefore, we infer that the arsenopyrite precipitation might have taken place at 1830 Ma at the earliest. Based on our age data we suggest two gold mineralising hydrothermal events at (I) ca. 1815–1805 Ma and (II) ca. 1795–1785 Ma in the study area (Fig. 13). Stage I is related to the second group foliation-parallel and gently crosscutting quartz veins and is characterised by precipitation of abundant arsenopyrite. The gold occurs as inclusions within arsenopyrites and has up to 10 % of Ag (Kärkkäinen et al., 2012). In Kultakallio stage I is prominently related to sub-conformable quartz veins (Kärkkäinen et al., 2016). Moreover, abundant arsenopyrite suggests low fO_2 and high As concentration of ore-forming fluids (e.g., Zhang and Zhu, 2021). Stage II is characterised by precipitation of native gold associated with Te- and Bi-minerals and abundant graphite (in Kultakallio; Fig. 10A). (Re-)Mobilisation of stage I Au is also likely during stage II (Kärkkäinen et al., 2012). Moreover, we suggest that the group three quartz-veins are related to stage II. This is based on the occurrence of narrow quartz-veins and graphite within broken and altered parts of arsenopyrites (Fig. 10A) and mobilisation of pyrite and chalcopyrite along small fault planes (Fig. 7C and F). Finally, zonation in gold grains and Ag-rich cores surrounded by Au-only rims also suggests two stage precipitation (Kärkkäinen et al., 2012).

The source and composition of the gold bearing fluids are still unclear. Interestingly the sheared, altered and sulphide rich-parts of the Kultakallio gabbro contains graphite (Fig. 9), which suggest a hydrothermal origin for the graphite, low fO_2 and CO_2-rich fluid for the stage II fluid pulses. Hydrothermal graphite has been identified in many orogenic gold deposits (e.g., Pitcairn et al., 2005; Hu et al., 2017) and Li et al., (2023) suggested that precipitation of hydrothermal graphite acts as a trigger for gold precipitation in *meso*-hypothermal gold deposits. Occurrence of graphite also suggests that the source of the fluid was the surrounding supracrustal rocks and fluids are metamorphic by origin

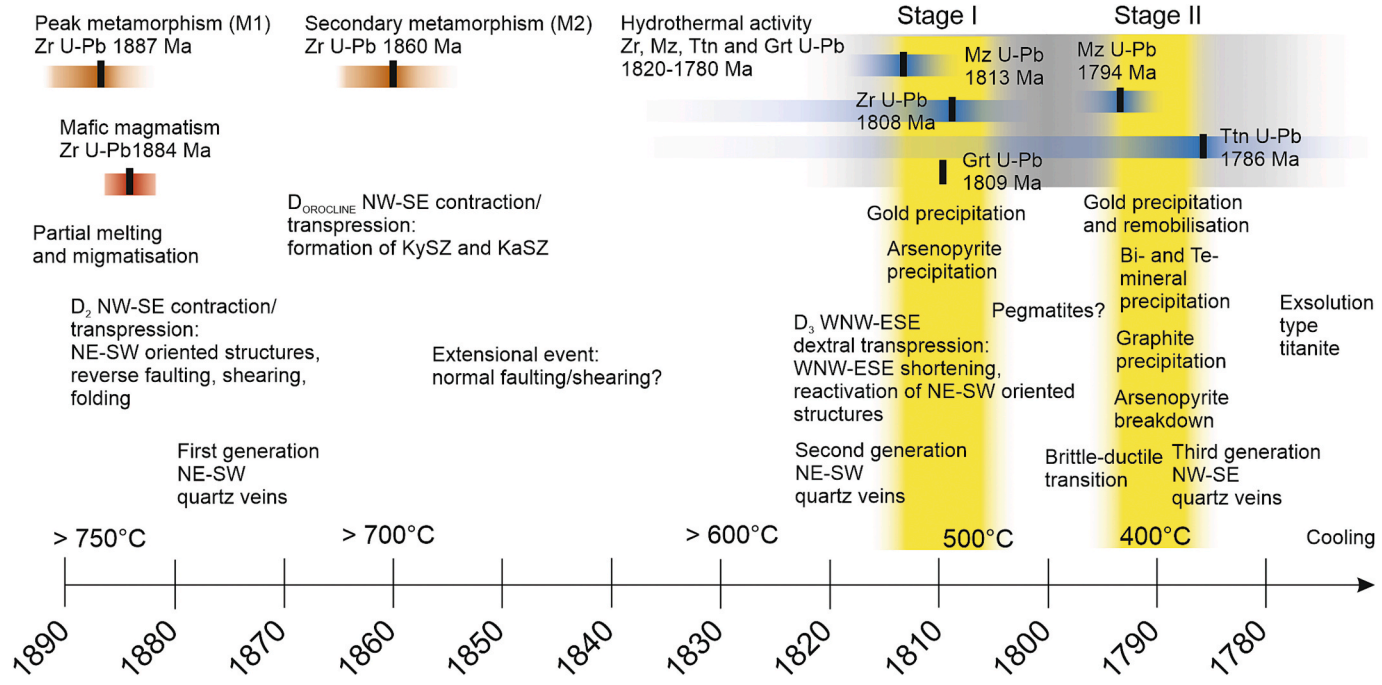

Fig. 13. Compilation of the obtained age data, timing of the deformation and mineralisation events in the Kullaa area. The location of the individual text boxes indicates approximately their age. Brown colour indicates metamorphism, red magmatism and blue hydrothermal activity. (For interpretation of the references to colour in this figure legend, the reader is referred to the web version of this article.)

rather than magmatic. However, many of the gold deposits in SW Finland are spatio-temporally associated with pegmatites (e.g., Eilu et al., 2003; Saalmann et al., 2009) and multiple pegmatite bodies occur in the study area as well. In addition, post-orogenic magmatism between 1.815 and 1.760 Ga (peaking at 1.80 Ga) is a widespread in the Svecofennian Orogen (Teräs et al., 2024) and these intrusions roughly occur in the same regions as orogenic gold deposits. This might suggest a link between hydrothermal activity, pegmatites and post-orogenic magmatism and thus the (partly) magmatic origin for the gold-bearing fluids cannot be fully ruled out.

5.4. Driver for the fluid activity

Results of age determinations addressing hydrothermal activity and gold precipitation within the Svecofennian crust (e.g., Saalmann et al., 2009; Saalmann et al., 2010; Molnár et al., 2018; Cutts et al., 2024; Kara et al., 2024; Vehkamäki et al., 2024) suggests that a substantial fluid pulse at roughly 1.8 Ga was a shield-wide event. This late-Svecofennian event is recognised in gold deposits in the Pirkanmaa and Häme belts (Saalmann et al., 2010) and also in other localities in Finland and Sweden, e.g. in the Kolari area (Niiranen et al., 2007), Norbotten area (Billström et al., 2002), Skellefte (Bark and Weihed, 2012), CLGB (Molnár et al., 2018) and even in places in the Archean basement (Cutts et al., 2024). This makes it one of the major ore forming periods in the Fennoscandian Shield since most of the orogenic gold deposits (e.g., Eilu et al., 2003, Saalmann et al., 2009; Molnár et al., 2018) and LCT pegmatites were formed during this time (Alviola et al., 2001).

The cause of this fluid activity is still obscure. Saalmann et al., (2009) suggested a model based on tectonic switching cycle (for further details see Collins, 2002) in which short contractional periods are followed by longer extensional events due to outboard migration of the subduction hinge in an active continental margin setting (Hermansson et al., 2008). In more detail, Saalmann et al., (2009) described transtension taking place between 1.86 and 1.83 Ga followed by transpression and crustal thickening during 1.83–1.80 Ga and finally slab break-off and upwelling of the asthenosphere occurred leading to post-tectonic magmatism and hydrothermal activity after 1.80 Ga. Another model involves orogenic/gravitational collapse, which has been suggested by several authors to occur broadly after 1.80 Ga (e.g., Korja et al., 2006). This model is based on thickening of the crust due to collisional tectonics during 1.84–1.80 Ga leading to subsequent gravitational collapse. Although, this model has not been directly correlated to gold mineralisation in Svecofennian orogen, the timing of the collapse and fluid activity matches. A similar model with post-collisional decompression and mantle delamination during the post-orogenic stage accounts for the prolonged hydrothermal activity and multiple mineralisations in the São Francisco craton, SE Brazil, which shows similar high T low P metamorphism as that in SW Finland (Gonçalves et al., 2019).

These two models have essential differences in their pre 1.80 Ga evolution but both models involve extensional tectonics associated with hydrothermal activity taking place broadly at 1.80 Ga and as such are difficult to distinguish from each other. Moreover, both models involve crustal thickening and granulite facies metamorphism in the Uusimaa belt between 1.83 and 1.80 Ga although the tectonic setting is different. The crucial difference in the models is the general cause for the metamorphism since in the tectonic switching model it is related to extension, crustal thinning and heat from the asthenosphere whereas in the orogenic collapse model it is correlated with collisional tectonics and crustal thickening. Recently, Teräs et al. (2024) proposed a model – combining aspects of the two above mentioned models – for the post-orogenic magmatism during 1.815–1.76 Ga involving lower crustal eclogitisation, delamination coupled with slab breakoff and highlighting the effect of the subducting plate within the Transscandinavian Igneous Belt (TIB; Fig. 1A). These processes would provide also a possible source and engine for the fluid activity. We prefer the model by Saalmann et al, (2009) and Teräs et al., (2024) for the Svecofennian evolution between 1.86 and 1.78 Ga, which better explains the multiple (high T-low P) metamorphic peaks identified in SW Finland and their likely association with extensional tectonics (e.g., Kara et al., 2020; 2021) as well as the necessity for available hydrous fluids.

6. Conclusions

- The 1.885 Ga event represents peak metamorphism, partial melting and magmatism, the 1.86 Ga event represents a secondary metamorphism whereas the 1.815–1.78 Ga events comprise merely hydrothermal activities in the study area.
- Two gold mineralising hydrothermal events at (I) ca. 1815–1805 Ma and (II) ca. 1795–1785 Ma are recognised in the study area. Stage I is related to the injection of foliation-parallel quartz veins and is characterised by the precipitation of abundant arsenopyrite in which gold occurs as inclusions. Stage II is characterised by precipitation of native gold associated with Te- and Bi-minerals, abundant graphite and (re)mobilisation of pyrite and breakdown of arsenopyrite and is suggested to take place within the brittle-ductile boundary.
- The NW-SE −oriented transpressional setting formed the NE-SW −oriented gold critical structures originally at 1.89–1.88 Ga and these were later reactivated in the 1.83–1.78 Ga WNW-ESE transpressional setting.
- The NW-SE trending crustal scale shear zones, bordering the study area, are suggested to have formed approximately at 1.87–1.86 Ga. These shear zones are suggested to play a major role in fluid flow and as first order structures whereas the NE-SW oriented strike-slip structures form the second order structural setting. At target scale, foliation parallel and intersecting quartz veins and narrow shear zones represent the third order structures hosting the mineralisations.
- The driver for the fluid activity approximately at 1.80 Ga is lower crustal/upper mantle delamination during crustal extension in a tectonic switching cycle.

CRediT authorship contribution statement

Jaakko Kara: Writing – review & editing, Writing – original draft, Visualization, Project administration, Investigation, Funding acquisition, Conceptualization. **Jukka Manninen:** Writing – original draft, Visualization, Investigation. **Pietari Skyttä:** Writing – review & editing, Writing – original draft, Project administration, Investigation, Funding acquisition, Conceptualization. **Markku Väisänen:** Writing – review & editing, Writing – original draft, Project administration, Investigation, Funding acquisition, Conceptualization. **Hugh O'Brien:** Writing – review & editing, Investigation. **Kathryn Cutts:** Writing – review & editing, Investigation. **Paavo Nikkola:** Writing – review & editing, Investigation.

Declaration of competing interest

The authors declare that they have no known competing financial interests or personal relationships that could have appeared to influence the work reported in this paper.

Acknowledgements

This study was funded by the Geological Survey of Finland through the collaborative TYTY-project and by J. Kara's personal grant from the K.H. Renlund foundation. Arto Peltola is thanked for preparing the thin sections and the epoxy mount. Sören Frödjö is thanked for the help with SEM imagining and micro-XRF analyses. Two anonymous reviewers are thanked for their helpful comments for improving the manuscript.

Appendix A. Supplementary material

Supplementary data to this article can be found online at https://doi.org/10.1016/j.precamres.2025.107828.

Data availability

I have shared the data at the Attach file step

References

Akkerman, J. H., 2015. Seinäjoki Gold Project. Geological Survey of Finland, Relinquishment Report 2009-2014, 12p.

Alviola, R., Mänttäri, I., Mäkitie, H., Vaasjoki, M., 2001. Svecofennian rare-element granitic pegmatites of the Ostrobothnia region, western Finland: their metamorphic environment and time of intrusion. Geol. Surv. Finland Spec. Pap. 30, 9–29.

Bark, G., Weihed, P., 2007. Orogenic gold in the new Lycksele–Storuman ore province, northern Sweden; the Palaeoproterozoic Fäboliden deposit. Ore Geol. Rev. 32, 431–451. https://doi.org/10.1016/j.oregeorev.2007.01.001.

Bark, G., Weihed, P., 2012. Geodynamic settings for Paleoproterozoic gold mineralization in the Svecofennian domain: a tectonic model for the Fäboliden orogenic gold deposit, northern Sweden. Ore Geol. Rev. 48, 403–412. https://doi.org/10.1016/j.oregeorev.2012.05.007.

Bedrock of Finland – DigiKP, 2024. Digital map database [electronic resource]. Espoo: Geological Survey of Finland [referred 1.7.2024] Version 2.1.

Bergman, S., Högdahl, K., Nironen, M., Ogenhall, E., Sjöström, H., Lundqvist, L., Lahtinen, R., 2008. Timing of Palaeoproterozoic intra-orogenic sedimentation in the central Fennoscandian Shield; evidence from detrital zircon in metasandstone. Precambr. Res. 161, 231–249. https://doi.org/10.1016/j.precamres.2007.08.007.

Billström, K., Bergman, S., Martinsson, O., 2002. Post-1.9 Ga metamorphic, mineralization and hydrothermal events in northern Sweden (Extended Abstract). GFF 124, 228.

Cherniak, D.J., Watson, E.B., 2001. Pb diffusion in zircon. Chem. Geol. 172, 5–24. https://doi.org/10.1016/S0009-2541(00)00233-3.

Cherniak, D.J., Watson, E.B., Grove, M., Harrison, T.M., 2004. Pb diffusion in monazite: a combined RBS/SIMS study. Geochimicaet Cosmochimica Acta 68, 829–840. https://doi.org/10.1016/j.gca.2003.07.012.

Chew, D.M., Spikings, R.A., 2021. Apatite U-Pb thermochronology: A review. Minerals 11, 1095. https://doi.org/10.3390/min11101095.

Chopin, F., Korja, A., Nikkilä, K., Hölttä, P., Korja, T., Abdel Zaher, M., Kurhila, M., Eklund, O., Rämö, O.T., 2020. The Vaasa Migmatitic Complex (Svecofennian Orogen, Finland): Buildup of a LP-HT Dome During Nuna Assembly. Tectonics 39, e2019TC005583. https://doi.org/10.1029/2019TC005583.

Collins, W.J., 2002. Hot orogens, tectonic switching, and creation of continental crust. Geology 30, 535–538. https://doi.org/10.1130/0091-7613(2002)030<0535:HOTSAC>2.0.CO;2.

Cutts, K. A., Szentpeteri, K., Karvinen, S., Glorie, S., Käpyaho, A., O'Brien, H., 2024. In situ Lu-Hf dating of garnet and apatite to understand fluid processes. In: Heinonen J. S., (Eds.), Abstract of the 2nd GeoDays, Turku, Finland. Proceedings of The Geological Society of Finland 4, 22.

Eilu, P., Sorjonen-Ward, P., Nurmi, P., Niiranen, T., 2003. A review of gold mineralization styles in Finland. Econ. Geol. 98, 1329–1353. https://doi.org/10.2113/gsecongeo.98.7.1329.

Eilu, P., 2012. Gold mineralisation in southwestern Finland. Geol. Surv. Finland Spec. Pap. 52, 11–22.

Engström, J., Cutts, K., Glorie, S., Heilimo, E., Jolis, E.M., Michallik, R.M., 2025. Insights into the tectonic evolution of the Svecofennian orogeny based on in situ Lu-Hf dating of garnet from Olkiluoto, SW Finland. Solid Earth 16, 97–117. https://doi.org/10.5194/se-16-97-2025.

Engström, J., Kärki, A., Paulamäki, S., Mänttäri, I., 2022. Palaeoproterozoic structural evolution of polyphase migmatites in Olkiluoto SW Finland. Bull. Geol. Soc. Finland 94, 119–144. https://doi.org/10.17741/bgsf/94.2.002.

Fitzsimons, I.C.W., Kinny, P.D., Wetherley, S., Hollingsworth, D.A., 2005. Bulk chemical control on metamorphic monazite growth in pelitic schists and implications for U–Pb age data. J. Metam. Geol. 23, 261–277. https://doi.org/10.1111/j.1525-1314.2005.00575.x.

Gaál, G., Gorbatschev, R., 1987. An outline of the Precambrian evolution of the Baltic Shield. Precambrian research 35, 15–52. https://doi.org/10.1016/0301-9268(87)90044-1.

Geisler, T., Schaltegger, U., Tomaschek, F., 2007. Re-equilibration of zircon in aqueous fluids and melts. Elements 3, 43–50. https://doi.org/10.2113/gselements.3.1.43.

Glorie, S., Hand, M., Mulder, J., Simpson, A., Emo, R.B., Kamber, B., Fernie, N., Nixon, A., Gilbert, S., 2024. In: van Schijndel, V., Cutts, K., Pereira, I., Guitreau, M., Volante, S., Tedeschi, M. (Eds.). https://doi.org/10.1144/SP537-2022-205.

Gonçalves, G.O., Lana, C., Buick, I.S., Alkmim, F.F., Scholz, R., Queiroga, G., 2019. Twenty million years of post-orogenic fluid production and hydrothermal mineralization across the external Araçuaí orogen and adjacent São Francisco craton, SE Brazil. Lithos 342, 557–572. https://doi.org/10.1016/j.lithos.2019.04.022.

Groves, D.I., Santosh, M., Deng, J., Wang, Q., Yang, L., Zhang, L., 2020. A holistic model for the origin of orogenic gold deposits and its implications for exploration. Mineralium Deposita 55, 275–292. https://doi.org/10.1007/s00126-019-00877-5.

Hector, S., Patten, C.G., Kolb, J., de Araujo Silva, A., Walter, B.F., Molnár, F., 2023. Orogenic Au deposits with atypical metal association (Cu, Co, Ni): Insights from the Pohjanmaa Belt, western Finland. Ore Geol. Rev. 154, 105326. https://doi.org/10.1016/j.oregeorev.2023.105326.

Hermann, J., Rubatto, D., 2003. Relating zircon and monazite domains to garnet growth zones: age and duration of granulite facies metamorphism in the Val Malenco lower crust. J. Metam. Geol. 21, 833–852. https://doi.org/10.1046/j.1525-1314.2003.00484.x.

Hermansson, T., Stephens, M.B., Corfu, F., Andersson, J., Page, L., 2007. Penetrative ductile deformation and amphibolite-facies metamorphism prior to 1851 Ma in the western part of the Svecofennian orogen, Fennoscandian Shield. Precambr. Res. 153, 29–45. https://doi.org/10.1016/j.precamres.2006.11.009.

Hermansson, T., Stephens, M.B., Corfu, F., Page, L.M., Andersson, J., 2008. Migratory tectonic switching, western Svecofennian orogen, central Sweden: Constraints from U/Pb zircon and titanite geochronology. Precambr. Res. 161, 250–278. https://doi.org/10.1016/j.precamres.2007.08.008.

Högdahl, K., Majka, J., Sjöström, H., Nilsson, K.P., Claesson, S., Konečný, P., 2012. Reactive monazite and robust zircon growth in diatexites and leucogranites from a hot, slowly cooled orogen: implications for the Palaeoproterozoic tectonic evolution of the central Fennoscandian Shield, Sweden. Contrib. Miner. Petrol. 163, 167–188. https://doi.org/10.1007/s00410-011-0664-x.

Hölttä, P., Väisänen, M., Väänänen, J., Manninen, T., 2007. Paleoproterozoic metamorphism and deformation in Central Lapland, Finland. Gold in the Central Lapland Greenstone Belt. Geol. Surv. Finland Spec. Pap. 44, 7–56.

Hölttä, P., Heilimo, E., 2017. Metamorphic Map of Finland. Bedrock of Finland at the scale 1:1000 000 – Major stratigraphic units, metamorphism and tectonic evolution. Geol. Surv. Finland Spec. Pap. 60, 77–128.

Hoskin, P.W., 2005. Trace-element composition of hydrothermal zircon and the alteration of Hadean zircon from the Jack Hills, Australia. Geochimicaet Cosmochimica Acta 69, 637–648. https://doi.org/10.1016/j.gca.2004.07.006.

Hu, S.Y., Evans, K., Craw, D., Rempel, K., Grice, K., 2017. Resolving the role of carbonaceous material in gold precipitation in metasediment-hosted orogenic gold deposits. Geology 45, 167–170. https://doi.org/10.1130/G38462.1.

Isomaa, J., Koistinen, E., Kärkkäinen, N., 2010. Sikakangas gold prospect at Seinäjoki, Western Finland. Geological Survey of Finland, Archive Report 55 (2010), 37p.

Janeczek, J., 1994. The effect of aluminous titanite on the biotite-chlorite and amphibole-chlorite reactions. Eur. J. Mineral. 6, 623–626. https://doi.org/10.1127/ejm/6/5/0623.

Johnson, A., Eklund, O., Heinonen, J. S., 2024. 1865 Ma Svecofennian mantle derived magmatism in Nagu, SW Finland. In: Heinonen J. S., (Eds.), Abstract of the 2nd GeoDays, Turku, Finland. Proceedings of The Geological Society of Finland 4, 31.

Kähkönen, Y., 2005. Svecofennian Supracrustal Rocks. Developments in Precambrian Geology 14, 343–405. https://doi.org/10.1016/S0166-2635(05)80009-X.

Kara, J., Väisänen, M., Johansson, Å., Lahaye, Y., O'Brien, H., Eklund, O., 2018. 1.90-1.88Ga arc magmatism of central Fennoscandia: Geochemistry, U-Pb geochronology, Sm-Nd and Lu-Hf isotope systematics of plutonic-volcanic rocks from southern Finland. GeologicaActa 16, 1–23. https://doi.org/10.1344/GeologicaActa2018.16.1.1.

Kara, J., Väisänen, M., Heinonen, J.S., Lahaye, Y., O'Brien, H., Huhma, H., 2020. Tracing arclogites in the Paleoproterozoic Era–A shift from 1.88 Ga calc-alkaline to 1.86 Ga high-Nb and adakite-like magmatism in central Fennoscandian Shield. Lithos 372, 105663. https://doi.org/10.1016/j.lithos.2020.105663.

Kara, J., Leskelä, T., Väisänen, M., Skyttä, P., Lahaye, Y., Tiainen, M., Leväniemi, H., 2021. Early Svecofennian rift-related magmatism: Geochemistry, U-Pb-Hf zircon isotope data and tectonic setting of the Au-hosting Uunimäki gabbro, SW Finland. Precambr. Res. 364, 106364. https://doi.org/10.1016/j.precamres.2021.106364.

Kara, J., O'Brien, H., Nikkola, P., Heilimo, E., Väisänen, M., 2024. Age determination of Au-precipitating fluid activity in SW Finland. In: Heinonen J. S., (Eds.), Abstract of the 2nd GeoDays, Turku, Finland. Proceedings of The Geological Society of Finland 4, 108.

Kärkkäinen, M., Lehto, T., Pakkanen, L., Rosenberg, P., 2012. Exploration and the mineralogy of gold in the Kullaa area, southwestern Finland. In: Grönholm, S., Kärkkäinen, N., (Eds.). Gold in Southern Finland: Results of GTK studies 1998–2011. Geological Survey of Finland, Special Paper 52, 131–148.

Kara, J., Väisänen, M., O'Brien, H., 2022. Zircon dating of the basalt and felsic dyke in Haveri, SW Finland. Bulletin of the Geological Society of Finland 94, 109–118. https://doi.org/10.17741/bgsf/94.2.001.

Kärkkäinen, N., Huhta, P., Al-Ani, T., 2015. Uunimäen kultaesiintymän malmimineralogia. Geol. Surv. Finland, Archive Report 76 (2015), 15p in Finnish.

Kärkkäinen, N., Huhta, P., Leväniemi, H., 2016. Kullaan vyöhykkeen malmipotentiaali, Saarijärven ja Kultakallion Au-mineralisaatiot. Geological Survey of Finland, Archive Report 75 (2016), 42p in Finnish.

Kelsey, D.E., Clark, C., Hand, M., 2008. Thermobarometric modelling of zircon and monazite growth in melt-bearing systems: Examples using model metapelitic and metapsammitic granulites. J. Metam. Geol. 26, 199–212. https://doi.org/10.1111/j.1525-1314.2007.00757.x.

Kilpeläinen, T., 1998. Evolution and 3D modelling of structural and metamorphic patterns of the Paleoproterozoic crust in the Tampere-Vammala area, southern Finland. Geol. Surv. Finland, Bulletin 397, 1–124.

Kohonen, J., Lahtinen, R., Luukas, J., Nironen, M., 2021. Classification of regional-scale tectonic map units in Finland. In: Kohonen, J., Tarvainen, T. (Eds.), Developments in map data management and geological unit nomenclature in Finland. Geological Survey of Finland, Bulletin 412, 33–81.

Koistinen, T., Stephens, M.B., Bogatchev, V., Nordgulen, Ø.,Wennerström, M., Korhonen, J., 2001. Geological map of the Fennoscandian Shield, scale 1:2000 000. Geological Surveys of Finland, Norway and Sweden and the North-West Department of Natural Resources of Russia.

Korja, A., Lahtinen, R., Nironen, M., 2006. The Svecofennian orogen: a collage of microcontinents and island arcs. Geol. Soc. Lond. Mem. 32, 561–578. https://doi.org/10.1144/GSL.MEM.2006.032.01.34.

Korsman, K., Koistinen, T., Kohonen, J., Wennerström, M., Ekdahl, E., Honkamo, M., Idman, H., Pekkala, Y., 1997. Suomen kallioperäkartta–Berggrundskarta över Finland–Bedrock map of Finland. Geological Survey of Finland, Espoo, Finland.

Lahtinen, R., 1996. Geochemistry of Palaeoproterozoic supracrustal and plutonic rocks in the Tampere-Hameenlinna area, southern Finland. Geol. Surv. Finland, Bulletin 389, 113p.

Lahtinen, R., Korja, A., Nironen, M., 2005. Paleoproterozoic tectonic evolution. Precambrian Geology of Finland 481–532. https://doi.org/10.1016/S0166-2635(05)80012-X.

Lahtinen, R., Huhma, H., Kähkönen, Y., Mänttäri, I., 2009. Paleoproterozoic sediment recycling during multiphase orogenic evolution in Fennoscandia, the Tampere and Pirkanmaa belts, Finland. Precambr. Res. 174, 310–336. https://doi.org/10.1016/j.precamres.2009.08.008.

Lahtinen, R., Nironen, M., 2010. Paleoproterozoic lateritic paleosol–ultra-mature/mature quartzite–meta-arkose successions in southern Fennoscandia—intra-orogenic stage during the Svecofennian orogeny. Precambr. Res. 183, 770–790. https://doi.org/10.1016/j.precamres.2010.09.006.

Lahtinen, R., Johnston, S.T., Nironen, M., 2014. The Bothnian coupled oroclines of the Svecofennian Orogen: a Palaeoproterozoic terrane wreck. Terra Nova 26, 330–335. https://doi.org/10.1111/ter.12107.

Lahtinen, R., Köykkä, J., Salminen, J., Sayab, M., Johnston, S.T., 2023. Paleoproterozoic tectonics of Fennoscandia and the birth of Baltica. Earth Sci. Rev. 104586. https://doi.org/10.1016/j.earscirev.2023.104586.

Lehto, T., Kärkkäinen, N., 2006. Tutkimustyöselostus Kullaan kunnassa valtausalueella Välimäki, kaivosrekisterinumero 7101/1, suoritetuista malmitutkimuksista. Geological Survey of Finland. Claim Report 12p in Finnish.

Li, W., Zhang, F., Qiao, X., Fu, T., 2023. Hydrothermal Graphite as a Trigger for High-Temperature Orogenic Gold Mineralization at Haoyaoerhudong, Northern China. Econ. Geol. 118, 1857–1880. https://doi.org/10.5382/econgeo.5018.

Ludwig, K.R., 2012. User's Manual for Isoplot 3.75, a geochronological toolkit for Microsoft Excel. Berkeley Geochronology Center Special Publication 5, 1–72.

Mänttäri, I., 1995. Lead isotope characteristics of epigenetic gold mineralization in the Palaeoproterozoic Lapland greenstone belt, northern Finland. Geol. Surv. Finland, Bulletin 381, 70p.

Mänttäri, I., Talikka, M., Paulamäki, S., and Mattila, J., 2006. U–Pb ages for tonalitic gneiss, pegmatitic granite, and diabase dyke, Olkiluoto study site, Eurajoki, SW Finland, Working Report No. 2006–12, Posiva Working Report, Posiva Oy, Eurajoki, https://www.posiva.fi/en/index/media/reports.html (last access: 3 February 2025).

Molnár, F., Middleton, A., Stein, H., Hugh, O., Lahaye, Y., Huhma, H., Johanson, B., 2018. Repeated syn-and post-orogenic gold mineralization events between 1.92 and 1.76 Ga along the Kiistala Shear Zone in the Central Lapland Greenstone Belt, northern Finland. Ore Geol. Rev. 101, 936–959. https://doi.org/10.1016/j.oregeorev.2018.08.015.

Molnár, F., Lahaye, Y., O'Brien, H., Kurhila, M., Hulkki, H., Demény, A., Richard, A., 2019. The Saattopora orogenic Au-Cu deposit, Central Lapland Greenstone belt, Finland: fluid sources and timing of hydrothermal processes. In: 15th SGA Biennal Meeting 2019 2, 723-726.

Mottram, C.M., Cottle, J.M., 2024. An electron backscatter diffraction study of monazite: Linking the time-deformation path. Chem. Geol. 122238. https://doi.org/10.1016/j.chemgeo.2024.122238.

Mouri, H., Korsman, K., Huhma, H., 1999. Tectono-metamorphic evolution and timing of the melting processes in the Svecofennian Tonalite-Trondhjemite Migmatite belt: An example from Luopioinen, Tampere area, southern Finland. Bull. Geol. Soc. Finl. 71, 31–56.

Niiranen, T., Poutiainen, M., Mänttäri, I., 2007. Geology, geochemistry, fluid inclusion characteristics, and U–Pb age studies on iron oxide–Cu–Au deposits in the Kolari region, northern Finland. Ore Geol. Rev. 30, 75–105. https://doi.org/10.1016/j.oregeorev.2005.11.002.

Nironen, M., 1989. The Tampere Schist Belt: structural style within an early Proterozoic volcanic arc system in southern Finland. Precambr. Res. 43, 23–40. https://doi.org/10.1016/0301-9268(89)90003-X.

Nironen, M., 1997. The Svecofennian Orogen: a tectonic model. Precambr. Res. 86, 21–44. https://doi.org/10.1016/S0301-9268(97)00039-9.

Nironen, M., 2017. Guide to the geological map of Finland – Bedrock 1:1 000 000. Geol. Surv. Finland Spec. Pap. 60, 41–76.

Pajunen, M., Airo, M.L., Elminen, T., Mänttäri, I., Niemelä, R., Vaarma, M., Wennerström, M., 2008. Tectonic evolution of the Svecofennian crust in southern Finland. Geol. Surv. Finland Spec. Pap. 47, 15–160.

Park, C., Song, Y., Chung, D., Kang, I.M., Khulganakhuu, C., Yi, K., 2016. Recrystallization and hydrothermal growth of high U–Th zircon in the Weondong deposit, Korea: record of post-magmatic alteration. Lithos 260, 268–285. https://doi.org/10.1016/j.lithos.2016.05.026.

Parrish, R.R., 1990. U–Pb dating of monazite and its application to geological problems. Can. J. Earth Sci. 27, 1431–1450. https://doi.org/10.1139/e90-152.

Pietikäinen, K., 1994. The geology of the Paleoproterozoic Pori Shear Zone. Michigan Tech, PhD thesis. 129p.

Pitcairn, I.K., Roberts, S., Teagle, D.A., Craw, D., 2005. Detecting hydrothermal graphite deposition during metamorphism and gold mineralization. J. Geol. Soc. London 162, 429–432. https://doi.org/10.1144/0016-764904-139.

Pokrovski, G.S., Kara, S., Roux, J., 2002. Stability and solubility of arsenopyrite, FeAsS, in crustal fluids. Geochimicaet Cosmochimica Acta 66, 2361–2378. https://doi.org/10.1016/S0016-7037(02)00836-0.

Reimers, S., Engström, J., Riller, U., 2018. The Kynsikangas shear zone, Southwest Finland: Importance for understanding deformation kinematics and rheology of lower crustal shear zones. Extended abstract, 10th Lithosphere Symposium, Institute of Seismology, University of Helsinki, Report S-67, 95-98.

Rutland, R.R., Williams, I.S., Korsman, K., 2004. Pre-1.91 Ga deformation and metamorphism in the Palaeoproterozoic Vammala Migmatite Belt, southern Finland, and implications for Svecofennian tectonics. Bull. Geol. Soc. Finl. 76, 93–140. https://doi.org/10.17741/bgsf/76.1-2.005.

Saalmann, K., 2007. Structural control on gold mineralization in the Satulinmäki and Riukka prospects, Häme Schist Belt, southern Finland. Bull. Geol. Soc. Finl. 79, 69–93. https://doi.org/10.17741/bgsf/79.1.004.

Saalmann, K., Mänttäri, I., Ruffet, G., Whitehouse, M.J., 2009. Age and tectonic framework of structurally controlled Palaeoproterozoic gold mineralisation in the Häme Belt of southern Finland. Precambr. Res. 174, 53–77. https://doi.org/10.1016/j.precamres.2009.06.005.

Saalmann, K., Mänttäri, I., Peltonen, P., Whitehouse, M.J., Grönholm, P., Talikka, M., 2010. Geochronology and structural relationships of mesothermal gold mineralisation in the Palaeoproterozoic Jokisivu prospect, southern Finland. Geol. Mag. 147, 551–569. https://doi.org/10.1017/S0016756809990628.

Schandl, E.S., Gorton, M.P., 2004. A textural and geochemical guide to the identification of hydrothermal monazite: criteria for selection of samples for dating epigenetic hydrothermal ore deposits. Econ. Geol. 99, 1027–1035. https://doi.org/10.2113/gsecongeo.99.5.1027.

Sharp, Z.D., Essene, E.J., Kelly, W.C., 1985. A re-examination of the arsenopyrite geothermometer; pressure considerations and applications to natural assemblages. Can. Mineral. 23, 517–534.

Sun, Z., Wang, J., Wang, Y., Long, L., Hu, Q., Wang, M., Xie, H., 2020. Two generations of garnets and their relevance for the hydrothermal fluid evolution of the Hongyuntan deposit. NW China. Ore Geology Reviews 122, 103513. https://doi.org/10.1016/j.oregeorev.2020.103513.

Suominen, V., 1988. Radiometric ages on zircons from a cogenetic gabbro and plagioclase porphyrite suite in Hyvinkää, southern Finland. Bull. Geol. Soc. Finl. 60, 135–140.

Teräs, O., Nikkilä, K., Mikkola, P., Kotilainen, A., Eklund, O., Rämö, O.T., 2024. Paleoproterozoic post-orogenic magmatism in southern Finland; geochemical, geochronological and Sr-Nd isotopic constraints on origin and magmatic evolution. Bull. Geol. Soc. Finl. 96, 135–160.

Tiainen, M., Molnar, F., Koistinen, E., 2013. The Cu-Mo-Au mineralization of the Paleoproterozoic Kedonojankulma intrusion, Häme Belt, Southern Finland. Proceedings of the 12th Biennial SGA Meeting 2, 892–895.

Tomkins, A.G., Frost, B.R., Pattison, D.R., 2006. Arsenopyrite melting during metamorphism of sulfide ore deposits. Can. Mineral. 44, 1045–1062. https://doi.org/10.2113/gscanmin.44.5.1045.

Väisänen, M., Johansson, Å., Andersson, U.B., Eklund, O., Hölttä, P., 2012. Palaeoproterozoic adakite-and TTG-like magmatism in the Svecofennian orogen, SW Finland. Geol. Acta 10, 351–371.

Väisänen, M., Kara, J., Penttinen, H., Lahaye, Y., O'Brien, H., Skyttä, P., 2021. U-Pb zircon dating of igneous rocks in the Salo area, SW Finland. Extended abstract, 11th Lithosphere Symposium, 151–154.

Vehkamäki, T., Väisänen, M., Kurhila, M., O'Brien, H., Hölttä, P., Syrjänen, J. K., 2021. Metamorphic zones in SW Finland: monazite and zircon U-Pb dating of leucosomes in paragneisses. Extended abstract, 11th Lithosphere Symposium, 139–142.

Vehkamäki, T., Väisänen, M., Kara, J., O'Brien, H., Hölttä, P., 2024. Sequential crystallization of zircon, monazite and xenotime in the cordierite-orthoamphibole rocks in Orijärvi, southern Finland. In: Heinonen J. S., (Eds.), Abstract of the 2nd GeoDays, Turku, Finland. Proceedings of The Geological Society of Finland 4, 59.

Zhai, W., Zhang, E., Zheng, S.Q., Santosh, M., Sun, X.M., Niu, H.C., Han, S.Y., 2022. Hydrothermal zircon: Characteristics, genesis and metallogenic implications. Ore Geol. Rev. 149, 105111. https://doi.org/10.1016/j.oregeorev.2022.105111.

Zhang, H., Zhu, Y., 2021. Textural, trace elemental and sulfur isotopic signatures of arsenopyrite and pyrite from the Mandongshan gold deposit (west Junggar, NW China): Implications for the conditions of gold mineralization. Ore Geol. Rev. 129, 103938. https://doi.org/10.1016/j.oregeorev.2020.103938.